Thermodynamic assessment of the V–O system

3 authors:

Yang Yang
Thermo-Calc Software AB, Sweden
5 PUBLICATIONS **20** CITATIONS

SEE PROFILE

Huahai Mao
KTH Royal Institute of Technology
68 PUBLICATIONS **641** CITATIONS

SEE PROFILE

Malin Selleby
KTH Royal Institute of Technology
104 PUBLICATIONS **1,593** CITATIONS

SEE PROFILE

Some of the authors of this publication are also working on these related projects:

Phase relations and thermodynamic modelling of oxide systems View project

prediction of glass forming ability of amorphous alloys View project

Thermodynamic assessment of the V–O system

Yang Yang [a,*], Huahai Mao [a,b], Malin Selleby [a]

[a] Department of Materials Science and Engineering, KTH Royal Institute of Technology, 100 44 Stockholm, Sweden
[b] Thermo-Calc Software AB, Norra Stationsgatan 93, 113 64 Stockholm, Sweden

ABSTRACT

The V–O system was thermodynamically assessed using the CALPHAD method. The available experimental data on thermodynamic and thermochemical properties as well as phase diagram information were critically examined and a self-consistent set of thermodynamic parameters was obtained. In total 20 phases were included in this binary system. Five among them were treated as solid solution phases within the framework of the compound energy formalism. The halite phase was modeled as $(V,V^{+2},V^{+3},Va)_1(O^{-2},Va)_1$ covering the solubility of both V and O. Thermodynamic descriptions of two different models for the corundum phase are presented, one of which is more complex to correctly take the defect mechanisms into account. The liquid phase was described by the ionic two-sublattice model with the formula $(V^{+2})_P(O^{-2},Va^{-Q}, VO_{1.5},VO_2, VO_{2.5})_Q$. The stoichiometric Magnéli phases V_nO_{2n-1} (n is an integer between 4 and 8) were modeled as $(V^{+3})_2(V^{+4})_{n-2}(O^{-2})_{2n-1}$. Using the present thermodynamic description reliable experimental phase diagram, thermodynamic and thermochemical data were well reproduced.

© 2015 Elsevier Ltd. All rights reserved.

1. Introduction

Vanadium alloys are promising wall material in nuclear fusion reactors. Due to the reaction between alloy and oxygen gas in the high temperature plasma, vanadium oxides tend to form on the alloy surface, which not only deteriorate the performance of the alloy, but also contaminate the high temperature plasma [1]. It is known that oxygen, as one of the light element impurities, can significantly modify phase equilibria in vanadium alloys. It can shift phase boundaries at very low levels of uptake [2], thus affecting the mechanical properties of the alloys.

Fundamental thermodynamic information on the V–O system is essential for vanadium alloy design and to understand practical vanadium metallurgical process. The present work attempts to develop a self-consistent thermodynamic database of all phases in the V–O system, which makes it possible to calculate phase diagram and thermodynamic properties. The description may also be used to extrapolate into multicomponent oxide systems for practical applications.

The complicated V–O system provides a challenging opportunity for application of the sophisticated Calphad method. The VO–VO$_{2.5}$ sub-system has already been optimized by Kang [3], using the modified quasichemical model for the liquid phase. However, their evaluation is limited to the oxygen rich phases.

The goal of the present work is to obtain a fully consistent thermodynamic description in the full composition range of the V–O system, where phases with lower oxygen content are also taken into account which was not the case in the previous study. The liquid phase is described by the ionic two-sublattice model [4,5] which has been widely used to describe the thermodynamic properties of ionized liquids, *e.g.* oxides, sulfides [6–12]. The solid phases are described using the compound energy formalism (CEF) [13].

2. Experimental data

2.1. Phase diagram data

Literature reviews for the V–O system were carried out by Wriedt [14] and Alcock [15]. The complication of this system attributes not only the existence of numerous phases but also the lack or some controversial experimental results. Here in this paper only information relevant to the present optimization is briefly reviewed.

The equilibrium solid phases in the V–O system according to Wriedt [14] are: α (body centered cubic), β (body centered tetragonal), γ (monoclinic), δ (face centered cubic, *i.e.* halite), δ′ (body centered tetragonal, *i.e.* V$_{52}$O$_{64}$), V$_2$O$_3$ (corundum), V$_3$O$_5$ (monoclinic), Magnéli phases V$_n$O$_{2n-1}$ where $n=4$, 5, 6, 7 and 8 (triclinic), β-VO$_2$(tetragonal), α-VO$_2$(monoclinic), V$_6$O$_{13}$ (monoclinic), V$_3$O$_7$ (monoclinic) and V$_2$O$_5$ (orthorhombic). A complete list of phases considered in this work can be found in Table 1 and Figs. 2–4.

* Corresponding author.
  E-mail address: yaya@kth.se (Y. Yang).

The α-phase is a solid solution phase with a body centered cubic structure. Several investigations [16–19] studied the solubility of oxygen in α-vanadium. Fair agreement has been achieved between these results in the temperature range of 1073–1473 K.

The β-phase has a wide range of homogeneity, which forms peritectically at 1938 K [17]. Previous studies [16,17,20] reported the vanadium-rich boundaries for the β-phase. As it is difficult to identify the β-phase towards the oxygen-rich boundaries, the phase boundaries are still not well established.

The γ-phase has the stoichiometry of V_2O, which was found to be formed by a peritectoid reaction at 1458 ± 10 K [17]. The composition range of the γ-phase is uncertain due to the limited experimental results.

It was proposed by Alexander [17] that the δ-phase has a congruent melting point at 2063 ± 10 K. This phase has been known for a long time to have a wide composition range. The phase boundaries for the δ-phase were also uncertain attributing to the controversial experimental results from different methods.

The δ′-phase was first reported by Bell [21]. Wriedt [14] confirmed that it is formed from a peritectoid reaction $\delta + V_2O_3 \rightarrow \delta'$. It is treated in the present assessment as a stoichiometric $V_{52}O_{64}$ phase considering that its solubility is negligible.

V_2O_3 with corundum structure is the most stable phase with the highest melting temperature in this system. Friederich et al. [22] first measured its melting temperature to be 2240 K. Later Wriedt [14] proposed that V_2O_3 melts congruently at 2230 K which was adopted in the present work.

V_3O_5 phase was first reported by Klemm [23] and its stoichiometry was confirmed by Andersson [24]. However, its melting behavior is not accurately studied due to lack of experimental evidence.

The Magnéli phases are important representatives of intermediate compounds with mixed valences of the parent metal. Melting type (congruent or incongruent) and temperature of triclinic V_nO_{2n-1} (n is an integer between 4 and 8) phases have not been experimentally confirmed yet. Phase equilibria with these phases can be referred to Kang's optimization of the $VO–VO_{2.5}$ system [3]. Monoclinic V_6O_{13} and V_3O_7 phases have been reported to exist between VO_2 and V_2O_5. Toda [25] proposed an eutectic reaction $L \rightarrow V_3O_7 + V_2O_5$. Kachi [26] and Suito [27] determined the liquidus in the composition range between VO_2 and V_2O_5 with obvious discrepancies between their results.

The VO_2-phase undergoes a polymorphic transition between monoclinic α-VO_2 and tetragonal β-VO_2 at 341 K [14]. The reliable melting temperature of β-VO_2 is reported in the range of 1815–1818 K [28,29]. Cook's work [28] suggested an incongruent melting of the β-VO_2 phase.

2.2. Thermodynamic data

Many investigations were carried out on thermodynamic properties of the vanadium oxides by EMF technique using solid electrochemical cells [18–20, 30–34, 37]. The equilibrium oxygen partial pressure over all stable phases from V_2O_3 to VO_2 at various temperatures has been experimentally determined by [35–38,65–67]. These measurements are reproduced using the present description, see Figs. 9 and 10.

Heat contents ($H_T–H_{298.15}$) of V_2O_3 were experimentally determined by [28,39]. As the description of V_2O_3 from SSUB5 for the corundum phase was slightly revised here, comparison between experimental data and calculated results is discussed in the following section.

The enthalpy of formation, $\Delta_f^0 H_{298}$, of the Magnéli phases has been experimentally determined [30,63] and the entropy of these phases was investigated by Vasil'eva et al. [40]. These data together with the critically reviewed ones by Brewer [41] were considered in the present assessment and the comparisons are given in Tables 3 and 4.

3. Thermodynamic models

All the solution phases in this system have been described using the CEF. All $°G$ values are given relative to H^{SER}, the enthalpy of the stable state of the elements at 298.15 K and 1 bar. Here SER (Stable Elements Reference) is used to denote this reference state. The thermodynamic descriptions of the pure stoichiometric phases VO, V_2O_3, VO_2 and V_2O_5 were taken from the SSUB5 database in the Thermo-Calc databank.

3.1. Liquid

The two-sublattice ionic liquid model developed within the frame of the CEF is used to describe the liquid phase. The model follows Temkin [42] assuming the existence of two sublattices with cations mixing on one and anions on the other. Charged vacancies were introduced on the anion sublattice to keep electroneutrality and to extend the description to a metallic liquid with only cations on the first sublattice, i.e. to the pure vanadium liquid in the present case.

Vanadium can exist as divalent, trivalent, quadrivalent and quinquevalent in aqueous solutions. Mittelstädt [43] studied the oxidation state of vanadium in pure VO_x melts. It was found that x is close to 2.5 in the range of oxygen partial pressure from 10^{-3} to 0.94 atm. The deviation from stoichiometric V_2O_5 indicates equilibrium between V^{+4} and V^{+5} ions [43], which supports the use of two neutral species VO_2 and $VO_{2.5}$. Moreover, stoichiometric V_2O_3 solid phase is the most stable one with the highest melting temperature. In summary, all the four valence states of vanadium are considered in the model. Therefore, the liquid phase is described as $(V^{+2})_P(O^{-2}, Va^{-Q}, VO_{1.5}, VO_2, VO_{2.5})_Q$, where P and Q are the number of sites on each sublattice. P and Q having the value of average charge on the other sublattice may vary with composition. In the present case $Q=2$ in the whole composition range. The molar Gibbs energy of the liquid phase is given by

$$G_m = y_{V^{+2}} y_{O^{-2}} {}^o G_{V^{+2}:O^{-2}} + Q\,(y_{V^{+2}} y_{Va^{-Q}} {}^o G_V + y_{VO_2} {}^o G_{VO_2}$$
$$+\ y_{VO_{1.5}} {}^o G_{VO_{1.5}} + y_{VO_{2.5}} {}^o G_{VO_{2.5}})$$
$$+\ QRT\,(y_{O^{-2}} \ln y_{O^{-2}} + y_{Va} \ln y_{Va} + y_{VO_2} \ln y_{VO_2}$$
$$+\ y_{VO_{1.5}} \ln y_{VO_{1.5}} + y_{VO_{2.5}} \ln y_{VO_{2.5}}) + {}^E G_m \qquad (1)$$

where the $°G$:s represent all the corner compounds of the model. $^oG_{V^{+2}:O^{-2}}$ and $^oG_{VO_2}$ were evaluated in the present work. $^oG_{VO_{2.5}}$ and $^oG_{VO_{1.5}}$ were taken from SSUB5 database while ^oG_V was the Gibbs energy of SER-V. The excess Gibbs energy term, ^EG_m, which depends on the interaction between the species within each sublattice is here given by

$$^E G_m = y_{V^{+2}} y_{O^{-2}} y_{Va} L_{V^{+2}:O^{-2},Va} + y_{V^{+2}} y_{O^{-2}} y_{VO_{1.5}} L_{V^{+2}:O^{-2},VO_{1.5}} \qquad (2)$$

in an attempt to use as few parameters as possible. Redlich–Kister expressions were used for the interaction parameters,

$$L_{V^{+2}:O^{-2},Va} = {}^0L + {}^1L\,(y_{O^{-2}} - y_{Va})$$
$$L_{V^{+2}:O^{-2},VO_{1.5}} = {}^0L \qquad (3)$$

3.2. Solid phases

Due to lack of reliable experimental data, the ordered low temperature phases, α′ and β′ mentioned in Wriedt [14], were ignored in the present assessment.

3.2.1. α-phase (BCC_A2)

Certain amount of oxygen dissolves into bcc vanadium forming the solid-solution phase, α. It is described using a two-sublattice model with metal atoms on the first sublattice and vacancies and oxygen on the second sublattice. The number of interstitial sites in BCC is 3. The phase is thus represented as $(V)_1(O,Va)_3$.

3.2.2. Halite (δ)

Halite has the stoichiometry of VO and crystallizes in the NaCl-type structure (Strukturbericht B1), which has the generic name halite. It has been shown experimentally that the halite phase can exist over a wide range of compositions other than the ideal 50 at% oxygen. Here the δ-phase is modeled with two sublattices, one for vanadium ions and the other for oxygen ions.

As vanadium has several valency states, one can compare with wüstite (also B1 structure) in Fe–O [44] to describe the stoichiometric deviation towards higher oxygen content. Dissolving oxygen in FeO causes oxidation of some Fe^{+2} into Fe^{+3} meanwhile some vacancies are introduced on the cation sublattice to keep the electroneutrality. This scheme would give the following model for the present VO halite phase:

$(V^{+2}, V^{+3}, Va)_1(O^{-2})_1$
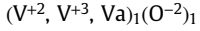
In the case of metallic V dissolving into the VO halite, *i.e.* stoichiometry deviations towards lower oxygen content, TiN (also B1 structure) [45] could be a comparable example where vacancy on the nitrogen sublattice gives a large composition range towards pure Ti. Similarly, in the present system the addition of metallic V is described by the introduction of Va on the oxygen sublattice and V (with zero valency) on the vanadium sublattice simultaneously. The introduction of Va on the oxygen sublattice reflects the oxygen-deficient condition while some V^{+2} is reduced into metallic V. To describe the solubility of both V and O into the VO halite, the following model is proposed:

$(V, V^{+2}, V^{+3}, Va)_1(O^{-2}, Va)_1$
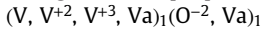
If the cation sublattice is denoted by I and the anion by II, the molar Gibbs energy of the halite phase according to the above model is expressed as follows

$$
\begin{aligned}
G_m =\ & y_V y_{O^{-2}}\, {}^oG_{V:O^{-2}} + y_V y_{Va}^{II}\, {}^oG_{V:Va} \\
& + y_{V^{+2}} y_{O^{-2}}\, {}^oG_{V^{+2}:O^{-2}} + y_{V^{+2}} y_{Va}^{II}\, {}^oG_{V^{+2}:Va} \\
& + y_{V^{+3}} y_{O^{-2}}\, {}^oG_{V^{+3}:O^{-2}} + y_{V^{+3}} y_{Va}^{II}\, {}^oG_{V^{+3}:Va} \\
& + y_{Va}^{I} y_{O^{-2}}\, {}^oG_{Va:O^{-2}} + y_{Va}^{I} y_{Va}^{II}\, {}^oG_{Va:Va} \\
& + RT(y_V \ln y_V + y_{V^{+2}} \ln y_{V^{+2}} + y_{V^{+3}} \ln y_{V^{+3}} \\
& + y_{Va}^{I} \ln y_{Va}^{I} + y_{O^{-2}} \ln y_{O^{-2}} + y_{Va}^{II} \ln y_{Va}^{II}) + {}^EG_m
\end{aligned} \tag{4}
$$

$$
\begin{aligned}
{}^EG_m =\ & y_V y_{V^{+2}} y_{O^{-2}} y_{Va}^{II} L_{V,V^{+2}:O^{-2},Va} + y_{V^{+2}} y_{V^{+3}} y_{O^{-2}} L_{V^{+2},V^{+3}:O^{-2}} \\
& + y_{V^{+3}} y_{O^{-2}} y_{Va}^{II} L_{V^{+3}:O^{-2},Va}
\end{aligned} \tag{5}
$$

The above Eq. (5) is the excess Gibbs energy which depends on the interaction between the species within each sublattice. Three interaction parameters were optimized in the present work.

This model is very complex as the same composition can be expressed in many different ways. Strict control must be applied to have a reasonable variation of the site fractions (see Fig. 7).

$L_{V,V^{+2}:O^{-2},Va}$ was evaluated to ensure the correct trend of V^{+2} replaced by V towards lower oxygen content than 50 at% while oxygen was replaced by vacancies on the second sublattice.

$L_{V^{+2},V^{+3}:O^{-2}}$ indicates the trend of V^{+3} and Va replacing V^{+2} towards higher oxygen content than 50 at%.

$L_{V^{+3}:O^{-2},Va}$ was used to enforce a low fraction of V^{+3} below 50 at% oxygen content.

Fig. 1 is a graphic representation of the halite phase model, where all eight end members are represented. Please note that V_2O_3 is not

an end-member but a stoichiometry which denotes the neutral combination of charged end-members $V^{+3}:O^{-2}$ and $Va:O^{-2}$. Red lines show the neutral surface connecting all neutral end members and combinations. ${}^oG_{V^{+2}:O^{-2}}$ and ${}^oG_{V:Va}$ are identical to the Gibbs energy of one mole of pure VO (GV1O1) and one mole of pure vanadium (GFCCVV), respectively. ${}^oG_{Va:O^{-2}}$ is chosen as the reference for the charged end-member of this halite phase. It can be given an arbitrary value and was set to zero here by convenience, which was explained in detail in [44]. ${}^oG_{Va:Va} = 30T$ is adopted from Thermo-Calc databank. The following equations were used:

$$
\begin{aligned}
{}^oG_{V^{+2}:O^{-2}} &= GV1O1 \\
{}^oG_{V:Va} &= GFCCVV \\
{}^oG_{Va:O^{-2}} &= 0 \\
{}^oG_{Va:Va} &= 30T
\end{aligned} \tag{6}
$$

The value of ${}^oG_{V^{+3}:O^{-2}}$ is optimized to fit the oxygen solubility based on the following equations

$$
\begin{aligned}
2\,{}^oG_{V^{+3}:O^{-2}} + {}^oG_{Va:O^{-2}} &= GV2O3 + A + B \cdot T \\
{}^oG_{V^{+3}:O^{-2}} &= 0.5\,GV2O3 + A' + B' \cdot T
\end{aligned} \tag{7}
$$

The Gibbs energy of the remaining three end-members can be derived assuming zero reaction energies of the reciprocal systems represented in Fig. 1.

$$
\begin{aligned}
{}^oG_{V:O^{-2}} &= GFCCVV - 30T \\
{}^oG_{V^{+2}:Va} &= GV1O1 + 30T \\
{}^oG_{V^{+3}:Va} &= 0.5\,GV2O3 + A' + B' \cdot T + 30T
\end{aligned} \tag{8}
$$

3.2.3. γ phase

The γ-phase is monoclinic and has been modeled having a similar Gibbs energy to the α phase with the interstitial sites occupied by oxygen [2]. In the present work it is modeled as $(V)_1(O, Va)_{0.5}$. The Gibbs energy is given by

$$
\begin{aligned}
G_m =\ & y_O\, {}^oG_{V:O} + y_{Va}\, {}^oG_{V:Va} + 0.5 \cdot RT(y_O \ln y_O + y_{Va} \ln y_{Va}) \\
& + y_O y_{Va} L_{V:O,Va}
\end{aligned} \tag{9}
$$

${}^oG_{V:O}$ was optimized in the present work while ${}^oG_{V:Va}$ is the Gibbs energy of vanadium in hcp structure.

3.2.4. β phase

The β-phase has a wide range of homogeneity. According to Hiraga [46], the β-phase has a BCT lattice for vanadium and the oxygen atoms are distributed preferentially in one of the three sets of octahedral interstitial sites. In CEF the site number of the interstitial oxygen sublattice is equal to 1. Therefore, the β-phase is modeled using the formula $(V)_1 (O, Va)_1$ and the G_m expression is written as
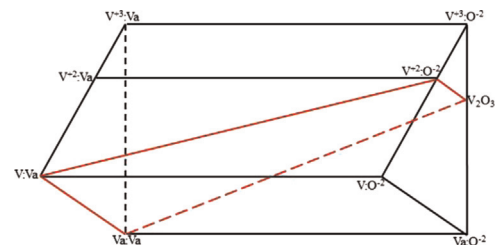

Fig. 1. The configurational compound energy model for the halite phase $(V, V^{+2}, V^{+3}, Va)_1(O^{-2}, Va)_1$. (For interpretation of the references to color in this figure, the reader is referred to the web version of this article.)

$$G_m = y_O \, {}^oG_{V:O} + y_{Va} \, {}^oG_{V:Va} + RT(y_O \ln y_O + y_{Va} \ln y_{Va})$$
$$+ y_O y_{Va} L_{V:O,Va} \tag{10}$$

${}^oG_{V:O}$ and ${}^oG_{V:Va}$ were optimized in the present work.

3.2.5. Corundum

Vanadium sesquioxide is a corundum phase with an ideal stoichiometry V_2O_3. It was found that vanadium sesquioxide exhibits considerable oxygen solubility [35,47]. Hence, the phase is simply described in the present work as $(V^{+3},V^{+4},Va)_2(O^{-2})_3$ in dataset 1, which could be used to model its non-stoichiometry. The following expression is the molar Gibbs energy of corundum,

$$^oG_m = y_{V^{+3}} \, {}^oG_{V^{+3}:O^{-2}} + y_{V^{+4}} \, {}^oG_{V^{+4}:O^{-2}} + y_{Va} \, {}^oG_{Va:O^{-2}}$$
$$+ 2RT(y_{V^{+3}} \ln y_{V^{+3}} + y_{V^{+4}} \ln y_{V^{+4}} + y_{Va} \ln y_{Va}) \tag{11}$$

The value of ${}^oG_{V^{+4}:O^{-2}}$ is optimized based on the following expression

$$^oG_{V^{+4}:O^{-2}} = GV2O3 + D + E{\cdot}T \tag{12}$$

where GV2O3 is the Gibbs energy of one mole of pure V_2O_3; D and E are parameters optimized here.

Non-stoichiometry of the V_2O_3 solid solution was observed toward the oxygen side. The defect could be excess oxygen, or metal deficiency, or a complex combination of both.

The above simple model (parameters in dataset 1) which only considers the metal deficiency gives reasonable thermodynamic descriptions except for the relations between oxygen partial pressure and defect concentration. Based on the available experimental data, Kang [3] analyzed the relations between oxygen partial pressure and defect concentration. The experimental data roughly shows that the logarithm of defect concentration looks proportional to $(p_{O2})^{1/2}$ at high oxygen partial pressure and proportional to (p_{O2}) at low oxygen partial pressure.

In the case of metal deficiency, neutral vacancy denotes the defect accounting for metal deficiency and V^{+4} denotes the vanadium atoms having the extra positive charge attributed to the defect. In the vicinity of stoichiometric V_2O_3 this model yields the following relation: $\log(y(Va,Corundum))$ is proportional to $\log(p_{O2})^{3/16}$. Here y(Va, Corundum) is the site fraction of vacancy which represents the defect concentration. Such an obtained proportionality of the defect concentration on the oxygen partial pressure is not consistent with the experimental data, thus the metal deficiency is not sufficient to interpret the defect mechanism of this phase.

In the case of excess oxygen, this phase can be modeled within the framework of CEF as $(V^{+3},V^{+4})_2(O^{-2})_3(Va,O^{-2})_1$, where the O^{-2} species in the third sublattice denotes the defects accounting for excess oxygen, i.e. extra oxygen dissolved on the interstitial sites (Va). Correspondingly certain amount of vanadium atoms is oxidized forming V^{+4} in the metal sublattice. This model yields the relation of $\log(y(O^{-2},Corundum))$ proportional to $\log(p_{O2})^{1/6}$. It turned out that excess oxygen alone is not sufficient either to interpret the defect mechanism of this phase.

Therefore, an advanced model which takes both metal deficiency and excess oxygen into account is needed. Assuming there is a strong interaction between the charged point defects V^{+4} and O^{-2} thus forming a defect "cluster", Kang [3] discussed an extended defect mechanism coupling the metal deficiency and excess oxygen. In CEF it could be described as $(V^{+3},V^{+4},Va)_2(O^{-2})_3(Va,O^{-2})_1$ which has the possibility to describe the slope of 1/2 between the logarithm of defect and oxygen partial pressure. In order to interpret the composition-dependent slope indicated by experimental information, Kang [3] emphasized an additional defect reaction $2V^{+3}=V^{+2}+V^{+4}$. In the present work, a complete thermodynamic model (parameters in dataset 2) becomes $(V^{+2},V^{+3},V^{+4},Va)_2(O^{-2})_3(Va,O^{-2})_1$.

There are eight end members. $(V^{+3})_2(O^{-2})_3(Va)_1$ stands for the stoichiometric V_2O_3. $(Va)_2(O^{-2})_3(Va)_1$ describes the metal deficiency mechanism. In CEF the ${}^oG$ value of this charged end member is set as a reference, by convenience, given the value zero. $(V^{+4})_2(O^{-2})_3(Va)_1$ counts in overall defect effect attributes to various mechanisms, which is the key parameter determining the homogeneity range of corundum, its Cp could be assumed identical to stoichiometric V_2O_3. $(V^{+2})_2(O^{-2})_3(Va)_1$ from the reaction of $2V^{+3}=V^{+2}+V^{+4}$ describes the composition-dependent slope, its Cp could also be assumed identical to stoichiometric V_2O_3. $(V^{+3})_2(O^{-2})_3(O^{-2})_1$ describes the excess oxygen mechanism, its Cp could be assumed identical to double that of VO_2. The ${}^oG$ value for the additional three end members can be derived assuming zero reciprocal reaction energy, i.e. $(V^{+4})_2(O^{-2})_3(O^{-2})_1$ from $(V^{+3},V^{+4})_2(O^{-2})_3(Va,O^{-2})_1$; $(Va)_2(O^{-2})_3(O^{-2})_1$ from $(V^{+4},Va)_2(O^{-2})_3(Va,O^{-2})_1$; and $(V^{+2})_2(O^{-2})_3(O^{-2})_1$ from $(V^{+2},V^{+4})_2(O^{-2})_3(Va,O^{-2})_1$. The following equations were used in the advanced model (dataset 2):

$$^0G_{Va:O^{-2}:Va} = 0$$
$$^0G_{V^{+4}:O^{-2}:Va} = GV2O3 + A'$$
$$^0G_{V^{+2}:O^{-2}:Va} = GV2O3 + B'$$
$$^0G_{V^{+3}:O^{-2}:O^{-2}} = 2GV1O2 + C'$$
$$^0G_{V^{+3}:O^{-2}:Va} = GV2O3 + D'$$
$$^0G_{V^{+2}:O^{-2}:O^{-2}} = 2GV1O2 + C' - D' + B'$$
$$^0G_{V^{+4}:O^{-2}:O^{-2}} = 2GV1O2 + C' + A' - D'$$
$$^0G_{Va:O^{-2}:O^{-2}} = 2GV1O2 + C' - D' - GV2O3 \tag{13}$$

where A', B', C' and D' are the parameters to be optimized.

3.2.6. Stoichiometric phases

The δ'-phase, the Magnèli phases, VO_2, V_3O_7, V_6O_{13} and V_2O_5, which do not exhibit detectable composition ranges due to the experimental uncertainties, are treated as stoichiometric phases in the present study. Their Gibbs energies are given by the following polynomials of the form

$$^oG - H^{SER} = A + BT + CT \ln T + ET^2 + FT^{-1} \tag{14}$$

An ordered phase (δ') which has a tetragonal structure with composition of $\sim V_{52}O_{64}$ is formed by long-term annealing of the superstoichiometric vanadium monoxide according to Andersson [48] and Morinaga [49].

The Magnéli phases could be described as recombination phases based on rebuilding after shear [50]. In the V–O system, the Magnéli series is formulated by a general representation V_nO_{2n-1} ($n=3–8$) between V_2O_3 and VO_2.

Glasser [51] studied the systematic thermodynamics of the vanadium oxide Magnéli phases. It was found in [51] that the Gibbs energy of formation for these phases varies in a systematic fashion across the whole composition range. An assumption of additivity for the values of thermodynamic quantities which were obtained by experiments is tested to be reliable [51]. Therefore, the Magnéli series V_nO_{2n-1} could be modeled as $V_nO_{2n-1}=V_2O_3 +(n-2){\cdot}VO_2$ ($n=3–8$), in a 3-sublattice CEF-model, $(V^{+3})_2(V^{+4})_{n-2}(O^{-2})_{2n-1}$.

It is found that there is a polymorphic transition for V_3O_5 at 428 K [14]. The high- and low-temperature polymorphic phases are denoted by V3O5_HT and V3O5_LT, respectively, corresponding to the two different monoclinic forms.

The VO_2-phase transforms between monoclinic α-VO_2 (denoted by VO2_LT here) and tetragonal β-VO_2 (denoted by VO2_HT here) at 341 K [14]. Both of them are described as $(V^{+4})_1(O^{-2})_2$.

Corresponding to polymorphic transitions of V_3O_5 and VO_2, the Gibbs energy expressions for the Magéli phases, V_3O_7 and V_6O_{13}, are divided into different temperature ranges.

According to the above mentioned generic thermodynamic model, the Gibbs energy expressions for the Magéli phases are given by

$$^{o}G_{V_3O_5\_LT} = {}^{o}G_{V_2O_3} + {}^{o}G_{VO_2\_LT} + X + Y \cdot T$$
$$^{o}G_{V_3O_5\_HT} = {}^{o}G_{V_3O_5\_LT} + U + V \cdot T \qquad (15)$$

when $n=3–8$, Gibbs energy is expressed as :

$$^{o}G_{V_nO_{2n-1}} = {}^{o}G_{V_3O_5\_LT} + (n-3) \cdot {}^{o}G_{VO_2\_LT} + A + B \cdot T \, (298.15 < T < 341)$$
$$^{o}G_{V_nO_{2n-1}} = {}^{o}G_{V_3O_5\_LT} + (n-3) \cdot {}^{o}G_{VO_2\_HT} + A + B \cdot T \, (341 < T < 428)$$
$$^{o}G_{V_nO_{2n-1}} = {}^{o}G_{V_3O_5\_HT} + (n-3) \cdot {}^{o}G_{VO_2\_HT} + A + B \cdot T \, (428 < T < 6000) \qquad (16)$$

Note: X, Y, U, V, A and B are parameters which were optimized in the present study. Here parameters A and B have different values for the respective phases.

Similarly, for the V_6O_{13} (monoclinic) and V_3O_7 (monoclinic), where vanadium has the valence between $+4$ and $+5$, were modeled as $V_nO_{2n+1}=V_2O_5+(n-2) \cdot VO_2$ ($n=3$ and 6), using a 3-sublattice model, $(V^{+5})_2 \, (V^{+4})_{n-2} \, (O^{-2})_{2n+1}$, which gives the following Gibbs energy expressions.

$$^{o}G_{V_3O_7} = {}^{o}G_{V_2O_5} + {}^{o}G_{VO_2\_LT} + M + N \cdot T \, (298.15 < T < 341)$$
$$^{o}G_{V_3O_7} = {}^{o}G_{V_2O_5} + {}^{o}G_{VO_2\_HT} + M + N \cdot T \, (341 < T < 6000)$$
$$^{o}G_{V_6O_{13}} = {}^{o}G_{V_2O_5} + 4 {}^{o}G_{VO_2\_LT} + J + K \cdot T \, (298.15 < T < 341)$$
$$^{o}G_{V_6O_{13}} = {}^{o}G_{V_2O_5} + 4 {}^{o}G_{VO_2\_HT} + J + K \cdot T \, ((341 < T < 6000) \qquad (17)$$

Note: M, N, J and K are parameters which were optimized in this work.

The V_2O_5-phase is modeled using the formula $(V^{+5})_2(O^{-2})_5$.

4. Optimization of parameters

The optimization was conducted using the PARROT module included in the Thermo-Calc software [52], which is able to consider all sorts of thermodynamic and phase diagram data simultaneously. During the assessment, the liquid phase was first introduced with interaction parameters $^{0}L^{Liq}_{V^{+2}:O^{-2}:Va}$ and $^{0}L^{Liq}_{V^{+2}O^{-2}:VO_{1.5}}$ to get a reasonable liquidus curve in the proper temperature range. Then α, β and γ phase were assessed considering the equilibrium oxygen partial pressure and phase diagram data while $^{1}L^{Liq}_{V^{+2}:O^{-2}:Va}$ was optimized to fit the invariant points L+α+β and L+β+halite. Thereafter the halite (δ) and corundum phase were included. Adjustments of the Gibbs energy for the end-members in Eq. (7) and Eq. (11) were made before the interaction parameters were added to fit the solubility. The corresponding parameters in liquid, halite and corundum were optimized together to fit the congruent melting and liquidus curve. Finally the Magnéli phases and other stoichiometric phases were added and their parameters optimized with particular attention to the experimental data of the equilibrium oxygen partial pressure. A final optimization was performed using all experimental information entered with proper weights and allowing changes of all parameters.

5. Results and discussion

A complete set of thermodynamic parameters describing the V–O system is given in Table 1. It should be mentioned here that the parameters for the rest of the phases are the same in the two datasets while those for the liquid and Magnéli phases are optimized corresponding to the different models for corundum.

Table 1
The thermodynamic properties of the V–O system (in SI units per mole of formula unit).

O$_2$-GAS

$$^{o}G^{O_2-GAS}_{O_2} - 2H^{SER}_O = \; + GO2GAS + RT \ln(P/1E5)$$

Liquid $(V^{+2})_P(O^{-2}, Va^{-Q}, VO_{1.5}, VO_2, VO_{2.5})_Q$

$$^{o}G^{Liq}_{V^{+2}:O^{-2}} - 2H^{SER}_V - 2H^{SER}_O = 2(GV1O1 + 94,854 - 46.53T)$$

$$^{o}G^{liq}_{V^{+2}:Va} - H^{SER}_V = GVLIQ$$

$$^{o}G^{Liq}_{VO_{1.5}} - H^{SER}_V - 1.5H^{SER}_O = 0.5GV2O3LIQ$$

$$^{o}G^{Liq}_{VO_2} - H^{SER}_V - 2H^{SER}_O = GV1O2LIQ + 3308.6$$

$$^{o}G^{Liq}_{VO_{2.5}} - H^{SER}_V - 2.5H^{SER}_O = 0.5GV2O5LIQ$$

$$^{0}L^{Liq}_{V^{+2}:O^{-2},Va} = -98,900$$
$$^{1}L^{Liq}_{V^{+2}:O^{-2},Va} = 51,034$$
$$^{0}L^{Liq}_{V^{+2}:O^{-2},VO_{1.5}} = 1449.9 - 50.71T \, (dataset1)$$
$$^{0}L^{Liq}_{V^{+2}:O^{-2},VO_{1.5}} = 61,786 - 78.47T \, (dataset2)$$

α phase (BCC_A2) $(V)_1(O,Va)_3$

$$^{o}G^{BCC}_{V:O} - H^{SER}_V - 3H^{SER}_O = GHSERVV + 1.5GO2GAS - 515,378 + 186.93T$$
$$^{o}G^{BCC}_{V:Va} - H^{SER}_V = GHSERVV$$
$$^{0}L^{BCC}_{V:O,Va} = -513,376$$
$$^{1}L^{BCC}_{V:O,Va} = 274,677$$

δ phase (Halite) $(V, V^{+2}, V^{+3}, Va)_1(O^{-2}, Va)_1$

$$^{0}G^{Hal}_{V:O^{-2}} - H^{SER}_V - H^{SER}_O = GFCCVV - 30T$$
$$^{o}G^{Hal}_{V:Va} - H^{SER}_V = GFCCVV$$
$$^{o}G^{Hal}_{V^{+2}:O^{-2}} - H^{SER}_V - H^{SER}_O = GV1O1$$
$$^{o}G^{Hal}_{V^{+2}:Va} - H^{SER}_V = GV1O1 + 30T$$
$$^{o}G^{Hal}_{V^{+3}:O^{-2}} - H^{SER}_V - H^{SER}_O = 0.5 \cdot GV2O3 + 10,956$$
$$^{o}G^{Hal}_{V^{+3}:Va} - H^{SER}_V = 0.5 \cdot GV2O3 + 10,956 + 30\,T$$
$$^{o}G^{Hal}_{Va:O^{-2}} - H^{SER}_O = 0$$
$$^{o}G^{Hal}_{Va:Va} = 30T$$
$$^{0}L^{Hal}_{V,V^{+2}:O^{-2},Va} = 37,205.229$$
$$^{0}L^{Hal}_{V^{+2},V^{+3}:O^{-2}} = -7958.4$$
$$^{0}L^{Hal}_{V^{+3}:O^{-2},Va} = 38,002$$

γ phase $(V)_1(O, Va)_{0.5}$

$$^{o}G^{\gamma}_{V:O} - H^{SER}_V - 0.5H^{SER}_O = GHCPVV + 0.25GO2GAS - 220,054 + 33.54T$$
$$^{o}G^{\gamma}_{V:Va} - H^{SER}_V = GHCPVV$$
$$^{0}L^{\gamma}_{V:O,Va} = -14,949$$

β phase $(V)_1(O, Va)_1$

Table 1 (*continued*)

$${}^oG^{\beta}_{V:O} - H^{SER}_V - H^{SER}_O = GV1O1 + 54,381 - 9.329T$$

$${}^oG^{\beta}_{V:Va} - H^{SER}_V = GHSERVV + 1540 - 0.512T$$

$${}^oL^{\beta}_{V:O,Va} = -101,228$$

Corundum (V_2O_3)
Simple model $(V^{+3}, V^{+4}, Va)_2(O^{-2})_3$
Dataset 1:

$${}^oG^{COR}_{V^{+3}:O^{-2}} - 2H^{SER}_V - 3H^{SER}_O = GV2O3 + 1150 - 15.5\,T$$

$${}^oG^{COR}_{Va:O^{-2}} - 3H^{SER}_O = 0$$

$${}^oG^{COR}_{V^{+4}:O^{-2}} - 2H^{SER}_V - 3H^{SER}_O = GV2O3 - 88,764.\,2 - 79.89T$$

Advanced model $(V^{+2}, V^{+3}, V^{+4}, Va)_2(O^{-2})_3(Va, O^{-2})_1$
Dataset 2:

$${}^oG^{COR}_{V^{+2}:O^{-2}:O^{-2}} - 4H^{SER}_O - 2H^{SER}_V = 2\cdot GV1O2\_LT + 466.95 - 3835.11 + 637.92$$

$${}^oG^{COR}_{V^{+3}:O^{-2}:O^{-2}} - 4H^{SER}_O - 2H^{SER}_V = 2\cdot GV1O2\_LT + 466.95$$

$${}^oG^{COR}_{V^{+4}:O^{-2}:O^{-2}} - 4H^{SER}_O - 2H^{SER}_V = 2\cdot GV1O2\_LT + 466.95 - 3835.11 + 4927.13$$

$${}^oG^{COR}_{Va:O^{-2}:O^{-2}} - 4H^{SER}_O = 2\cdot GV1O2\_LT + 466.95 - 3835.11 - GV2O3$$

$${}^oG^{COR}_{V^{+2}:O^{-2}:Va} - 3H^{SER}_O - 2H^{SER}_V = GV2O3 + 637.92$$

$${}^oG^{COR}_{V^{+3}:O^{-2}:Va} - 3H^{SER}_O - 2H^{SER}_V = GV2O3 + 3835.11$$

$${}^oG^{COR}_{V^{+4}:O^{-2}:Va} - 3H^{SER}_O - 2H^{SER}_V = GV2O3 + 4927.13$$

$${}^oG^{COR}_{Va:O^{-2}:Va} - 3H^{SER}_O = 0$$

δ'phase $(\mathbf{V_{52}O_{64}})(V)_{52}(O)_{64}$

$${}^oG^{\delta'}_{V:O} - 52H^{SER}_V - 64H^{SER}_O = 64\cdot GV1O1 - 12\cdot GFCCVV + 345,671 - 25T$$

V₃O₅_LT $(V^{+3})_2(V^{+4})_1(O^{-2})_5$

$${}^oG^{V_3O_5-LT}_{V^{+3}:V^{+4}:O^{-2}} - 3H^{SER}_V - 5H^{SER}_O = GV3O5\_LT$$

V₃O₅_HT $(V^{+3})_2(V^{+4})_1(O^{-2})_5$

$${}^oG^{V_3O_5-HT}_{V^{+3}:V^{+4}:O^{-2}} - 3H^{SER}_V - 5H^{SER}_O = GV3O5\_HT$$

V₄O₇ $(V^{+3})_2(V^{+4})_2(O^{-2})_7$

$${}^oG^{V_4O_7}_{V^{+3}:V^{+4}:O^{-2}} - 4H^{SER}_V - 7H^{SER}_O = GV4O7$$

V₅O₉ $(V^{+3})_2(V^{+4})_3(O^{-2})_9$

$${}^oG^{V_5O_9}_{V^{+3}:V^{+4}:O^{-2}} - 5H^{SER}_V - 9H^{SER}_O = GV5O9$$

V₆O₁₁ $(V^{+3})_2(V^{+4})_4(O^{-2})_{11}$

$${}^oG^{V_6O_{11}}_{V^{+3}:V^{+4}:O^{-2}} - 6H^{SER}_V - 11H^{SER}_O = GV6O11$$

V₇O₁₃ $(V^{+3})_2(V^{+4})_5(O^{-2})_{13}$

$${}^oG^{V_7O_{13}}_{V^{+3}:V^{+4}:O^{-2}} - 7H^{SER}_V - 13H^{SER}_O = GV7O13$$

V₈O₁₅ $(V^{+3})_2(V^{+4})_6(O^{-2})_{15}$

$${}^oG^{V_8O_{15}}_{V^{+3}:V^{+4}:O^{-2}} - 8H^{SER}_V - 15H^{SER}_O = GV8O15$$

Table 1 (*continued*)

VO₂_HT $(V^{+4})_1(O^{-2})_2$

$${}^oG^{VO_2-HT}_{V^{+4}:O^{-2}} - H^{SER}_V - 2H^{SER}_O = GV1O2\_HT$$

VO₂_LT $(V^{+4})_1(O^{-2})_2$

$${}^oG^{VO_2-LT}_{V^{+4}:O^{-2}} - H^{SER}_V - 2H^{SER}_O = GV1O2\_LT$$

V₃O₇ $(V^{+5})_2(V^{+4})_1(O^{-2})_7$

$${}^oG^{V_3O_7}_{V^{+5}:V^{+4}:O^{-2}} - 3H^{SER}_V - 7H^{SER}_O = GV3O7$$

V₆O₁₃ $(V^{+5})_2(V^{+4})_4(O^{-2})_{13}$

$${}^oG^{V_6O_{13}}_{V^{+5}:V^{+4}:O^{-2}} - 6H^{SER}_V - 13H^{SER}_O = GV6O13$$

V₂O₅ $(V^{+5})_2(O^{-2})_5$

$${}^oG^{V_2O_5}_{V^{+5}:O^{-2}} - 2H^{SER}_V - 5H^{SER}_O = GV2O5$$

Functions

GO2GAS $(298.15 < T < 900.00) = -6960.69252 - 51.1831473T - 22.25862T \ln T - 0.01023867T^2 + 1.339947 \times 10^{-6}T^3 - 76749.55T^{-1}$

GO2GAS $(900.00 < T < 3700.00) = -13,136.0172 + 24.743296T - 33.55726T \ln T - 0.0012348985T^2 + 1.66943333 \times 10^{-8}T^3 + 539,886T^{-1}$

GO2GAS $(3700.00 < T < 6000.00) = 14,154.6461 - 51.4854586T - 24.47978T \ln T - 0.0026347597T^2 + 6.01544333 \times 10^{-8}T^3 - 15,120,935T^{-1}$

GV1O1 $(298.15 < T < 2063.00) = -452,649.127 + 334.032868T - 52.91877T \ln T - 0.006557147T^2 + 5.33969167 \times 10^{-11}T^3 + 818,200T^{-1}$

GV1O1 $(2063.00 < T < 6000.00) = -459,188.444 + 454.230294T - 70T \ln T$

GVLIQ $(298.15 < T < 790.00) = 12,833.687 + 123.890501T - 24.134T \ln T - 0.003098T^2 + 1.2175 \times 10^{-7}T^3 - 5.19136 \times 10^{-22}T^7 + 69,460T^{-1}$

GVLIQ $(790.00 < T < 2183.00) = 12,796.275 + 133.835541T - 25.9T \ln T + 6.25 \times 10^{-5}T^2 - 6.8 \times 10^{-7}T^3 - 5.19136 \times 10^{-22}T^7$

GVLIQ $(2183.00 < T < 6000.00) = -19,617.51 + 311.055983T - 47.43T \ln T$

GV1O2LIQ $(298.15 < T < 340.00) = -666,043.928 + 104.5557163T - 23.84754T \ln T - 0.0754984T^2 + 1.68293667 \times 10^{-5}\,T^3 + 9,742.025T^{-1}$

GV1O2LIQ $(340.00 < T < 700.00) = -678,763.718 + 382.8539233T - 69.68954T \ln T - 0.008449182T^2 + 9.50542 \times 10^{-7}\,T^3 + 628,472.5T^{-1}$

GV1O2LIQ $(700.00 < T < 1400.00) = -680,716.919 + 410.4175703T - 73.9568T \ln T - 0.00370019825T^2 - 1.03988433 \times 10^{-7}\,T^3 + 822,530.5T^{-1}$

GV1O2LIQ $(1400.00 < T < 1818.00) = -676,412.045 + 378.7739833T - 69.61465T \ln T - 0.005721857T^2 + 8.000575 \times 10^{-8}T^3$

GV1O2LIQ $(1818.00 < T < 6000.00) = -725,868.707 + 674.1237373T - 106.692T \ln T$

GV2O3LIQ $(298.15 < T < 2230.00) = -1130,647.05 + 823.5539089T - 144.3096T \ln T + 0.00933134T^2 - 1.81532333 \times 10^{-6}\,T^3 + 1,722,474T^{-1}$

GV2O3LIQ $(2230.00 < T < 6000.00) = -1170233.34 + 974.4026209T - 160T \ln T$

GV2O5LIQ $(298.15 < T < 954.00) = -1,553,720.68 - 1079.37776611T - 190.8802T \ln T + 0.046392467T^2 - 1.58726633 \times 10^{-5}\,T^3 + 1,951,745.5T^{-1}$

GV2O5LIQ $(954.00 < T < 6000.00) = -1,563,448.88 + 1,115.4932261T - 190T \ln T$

GHSERVV $(298.15 < T < 790.00) = -7930.43 + 133.346053T - 24.134T \ln T - 0.003098T^2 + 1.2175 \times 10^{-7}T^3 + 69,460T^{-1}$

GHSERVV $(790.00 < T < 2183.00) = -7967.842 + 143.291093T - 25.9T \ln T + 6.25 \times 10^{-5}T^2 - 6.8 \times 10^{-7}T^3$

GHSERVV $(2183.00 < T < 6000.00) = -41,689.864 + 321.140783T - 47.43T \ln T + 6.44389 \times 10^{31}T^{-9}$

GFCCVV $(298.15 < T < 790.00) = -430.43 + 135.046053T - 24.134T \ln T - 0.003098T^2 + 1.2175 \times 10^{-7}T^3 + 69,460T^{-1}$

GFCCVV $(790.00 < T < 2183.00) = -467.842 + 144.991093T - 25.9T \ln T + 6.25 \times 10^{-5}T^2 - 6.8 \times 10^{-7}T^3$

GFCCVV $(2183.00 < T < 6000.00) = -34,189.864 + 322.840783T - 47.43T \ln T + 6.44389 \times 10^{31}T^{-9}$

GV1O1 $(298.15 < T < 2063.00) = -452,649.127 + 334.032868T - 52.91877T \ln T - 0.006557147T^2 + 5.33969167 \times 10^{-11}\,T^3 + 818,200T^{-1}$

GV1O1 $(2063.00 < T < 6000.00) = -459,188.444 + 454.230294T - 70T \ln T$

GV2O3 $(298.15 < T < 2230.00) = -1,270,647.05 + 886.334178T - 144.3096T \ln T + 0.00933134T^2 - 1.81532333 \times 10^{-6}\,T^3 + 1,722,474T^{-1}$

GV2O3 $(2230.00 < T < 6000.00) = -1,310,233.34 + 1,037.18289T - 160T \ln T$

GHCPVV $(298.15 < T < 790.00) = -3930.43 + 135.746053T - 24.134T \ln T - 0.003098T^2 + 1.2175 \times 10^{-7}T^3 + 69,460T^{-1}$

Table 1 (*continued*)

GHCPVV(790.00 < T < 2183.00) = $-3967.842 + 145.691093T - 25.9T$
　ln $T + 6.25 \times 10^{-5}T^2 - 6.8 \times 10^{-7}T^3$
GHCPVV(2183.00 < T < 6000.00) = $-37,689.864 + 323.540783T - 47.43T$ ln T
　$+ 6.44389 \times 10^{31}T^{-9}$
GV1O2_LT(298.15 < T < 340.00) = $-726,575.928 + 148.606432T - 23.84754T$
　ln $T - 0.0754984T^2 + 1.68293667 \times 10^{-5}\ T^3 + 9742.025T^{-1}$
GV1O2_LT(340.00 < T < 700.00) = $-739,295.718 + 426.904639T - 69.68954T$
　ln $T - 0.008841982T^2 + 9.50542 \times 10^{-7}\ T^3 + 628,472.5T^{-1}$
GV1O2_LT(700.00 < T < 1400.00) = $-741,248.919 + 454.468286T - 73.9568T$
　ln $T - 0.0037019825T^2 - 1.03988433 \times 10^{-7}\ T^3 + 822,530.5T^{-1}$
GV1O2_LT(1400.00 < T < 1818.00) = $-736,944.045 + 422.824699T - 69.61465T$
　ln $T - 0.00572185T^2 + 8.000575 \times 10^{-8}T^3$
GV1O2_LT(1818.00 < T < 6000.00) = $-786,400.707 + 718.174453T - 106.692T$ ln T
GV3O5_LT = GV2O3 + GV1O2_LT − 20,986 (dataset 1)
GV3O5_LT = GV2O3 + GV1O2_LT − 21,229 (dataset 2)
GV3O5_HT = GV2O3 + GV1O2_LT + 12,499.6 − 29.20T (dataset 1)
GV3O5_HT = GV2O3 + GV1O2_LT + 12,584.8 − 29.54T (dataset 2)
GV1O2_HT(298.15 < T < 340.00) = $-722,078.128 + 135.3776085T - 23.84754T$
　ln $T - 0.0754984T^2 + 1.68293667 \times 10^{-5}\ T^3 + 9742.025T^{-1}$
GV1O2_HT(340.00 < T < 700.00) = $-734,797.918 + 413.6758155T - 69.68954T$
　ln $T - 0.008841982T^2 + 9.50542 \times 10^{-7}\ T^3 + 628,472.5T^{-1}$
GV1O2_HT(700.00 < T < 1400.00) = $-736,751.119 + 441.2394625T - 73.9568T$
　ln $T - 0.0037019825T^2 - 1.03988433 \times 10^{-7}\ T^3 + 822,530.5T^{-1}$
GV1O2_HT(1400.00 < T < 1818.00) = $-$
　$732,446.245 + 409.5958755T - 69.61465T$ ln $T -$
　$0.00572185T^2 + 8.000575 \times 10^{-8}T^3$
GV1O2_HT(1818.00 < T < 6000.00) = $-781,902.907 + 704.9456295T - 106.692T$ ln T
GV4O7 (298.15 < T < 341.00) = GV3O5_LT + GV1O2_LT − 9979 + 3.13T (dataset 1)
GV4O7 (341.00 < T < 428.00) = GV3O5_LT + GV1O2_HT − 9979 + 3.13T (dataset 1)
GV4O7 (428.00 < T < 6000.00) = GV3O5_HT + GV1O2_HT − 9979 + 3.13T (dataset 1)
GV4O7 (298.15 < T < 341.00) = GV3O5_LT + GV1O2_LT − 9994 + 3.13T (dataset 2)
GV4O7 (341.00 < T < 428.00) = GV3O5_LT + GV1O2_HT − 9994 + 3.13T (dataset 2)
GV4O7 (428.00 < T < 6000.00) = GV3O5_HT + GV1O2_HT − 9994 + 3.13T (dataset 2)
GV5O9 (298.15 < T < 341.00) = GV3O5_LT + 2 GV1O2_LT − 16,919 + 6.29T (dataset 1)
GV5O9 (341.00 < T < 428.00) = GV3O5_LT + 2 GV1O2_HT − 16,919 + 6.29T (dataset 1)
GV5O9 (428.00 < T < 6000.00) = GV3O5_HT + 2 GV1O2_HT − 16,919 + 6.29T (dataset 1)
GV5O9 (298.15 < T < 341.00) = GV3O5_LT + 2 GV1O2_LT − 16,921 + 6.29T (dataset 2)
GV5O9 (341.00 < T < 428.00) = GV3O5_LT + 2 GV1O2_HT − 16,921 + 6.29T (dataset 2)
GV5O9 (428.00 < T < 6000.00) = GV3O5_HT + 2 GV1O2_HT − 16,921 + 6.29T (dataset 2)
GV6O11 (298.15 < T < 341.00) = GV3O5_LT + 3 GV1O2_LT − 23,149.4 + 9.56T (dataset 1)
GV6O11 (341.00 < T < 428.00) = GV3O5_LT + 3 GV1O2_HT − 23,149.4 + 9.56T (dataset 1)
GV6O11 (428.00 < T < 6000.00) = GV3O5_HT + 3 GV1O2_HT − 23,149.4 + 9.56T (dataset 1)
GV6O11 (298.15 < T < 341.00) = GV3O5_LT + 3 GV1O2_LT − 23,149.8 + 9.56T (dataset 2)
GV6O11 (341.00 < T < 428.00) = GV3O5_LT + 3 GV1O2_HT − 23,149.8 + 9.56T (dataset 2)
GV6O11 (428.00 < T < 6000.00) = GV3O5_HT + 3 GV1O2_HT − 23,149.8 + 9.56T (dataset 2)
GV7O13 (298.15 < T < 341.00) = GV3O5_LT + 4 GV1O2_LT − 24,034 + 10.172T (dataset 1)
GV7O13 (341.00 < T < 428.00) = GV3O5_LT + 4 GV1O2_HT − 24,034 + 10.172T (dataset 1)
GV7O13 (428.00 < T < 6000.00) = GV3O5_HT + 4 GV1O2_HT − 24,034 + 10.172T (dataset 1)
GV7O13 (298.15 < T < 341.00) = GV3O5_LT + 4 GV1O2_LT − 24,037 + 10.172T (dataset 2)
GV7O13 (341.00 < T < 428.00) = GV3O5_LT + 4 GV1O2_HT − 24,037 + 10.172T (dataset 2)
GV7O13 (428.00 < T < 6000.00) = GV3O5_HT + 4 GV1O2_HT − 24,037 + 10.172T (dataset 2)
GV8O15 (298.15 < T < 341.00) = GV3O5_LT + 5 GV1O2_LT − 24,398.9 + 10.447T (dataset 1)
GV8O15 (341.00 < T < 428.00) = GV3O5_LT + 5 GV1O2_HT − 24,398.9 + 10.447T (dataset 1)
GV8O15 (428.00 < T < 6000.00) = GV3O5_HT + 5
　GV1O2_HT − 24,398.9 + 10.447T (dataset 1)

Table 1 (*continued*)

GV8O15 (298.15 < T < 341.00) = GV3O5_LT + 5 GV1O2_LT − 24,401.8 + 10.447T
　(dataset 2)
GV8O15 (341.00 < T < 428.00) = GV3O5_LT + 5 GV1O2_HT − 24,401.8 + 10.447T
　(dataset 2)
GV8O15 (428.00 < T < 6000.00) = GV3O5_HT + 5
　GV1O2_HT − 24,401.8 + 10.447T (dataset 2)
GV2O5(298.15 < T < 954.00) = $-1,617,720.68 + 1,146.46372T - 190.8802T$
　ln $T + 0.04639246T^2 - 1.58726633 \times 10^{-5}\ T^3 + 1,951,745.5T^{-1}$
GV2O5(954.00 < T < 6000.00) = $-1,627,448.88 + 1182.57918T - 190T$ ln T
GV3O7(298.15 < T < 341.00) = GV2O5 + GV1O2_LT − 26,769 + 27.28T
GV3O7(341.00 < T < 6000.00) = GV2O5 + GV1O2_HT − 26,769 + 27.28T
GV6O13(298.15 < T < 341.00) = GV2O5 + 4 GV1O2_LT − 27,412 + 25.57T
GV6O13(341.00 < T < 6000) = GV2O5 + 4 GV1O2_HT − 27,412 + 25.57T

Table 2
Invariant equilibria in the V–O system.

| Reaction	Temperature (K)	X_O in phases	Reference
L + α → β	1938	$X(liq,O) = 0.27$ $X(\alpha,O) = 0.17$ $X(\beta,O) = 0.2$	Alexander [17]
	1980	$X(liq,O) = 0.2167$ $X(\alpha,O) = 0.1812$ $X(\beta,O) = 0.2007$	This work
L → β + halite	1913	$X(liq,O) = 0.29$ $X(\beta,O) = 0.205$ $X(hal,O) = 0.44$	Alexander [17]
	1888	$X(liq,O) = 0.3259$ $X(\beta,O) = 0.2726$ $X(hal,O) = 0.4339$	This work
β + halite → γ	1620	$X(\beta,O) = 0.275$ $X(hal,O) = 0.45$ $X(\gamma,O) = 0.3$	Davydov [53]
	1458	$X(\beta,O) = 0.286$ $X(hal,O) = 0.45$ $X(\gamma,O) = 0.333$	Wriedt [14]
	1590	$X(\beta,O) = 0.2724$ $X(hal,O) = 0.4508$ $X(\gamma,O) = 0.3107$	This work
L → halite	2063	–	Alexander [17]
	2046	–	Dataset 1
	2053	–	Dataset 2
Halite + corundum → δ′	1070	–	Davydov [53]
	1083	$X(cor,O) = 0.6$ $X(hal,O) = 0.56$ $X(\delta',O) = 0.57$	Wriedt [14]
	1063	$X(cor,O) = 0.6$ $X(hal,O) = 0.5466$ $X(\delta',O) = 0.5517$	Dataset 1
	1058	$X(cor,O) = 0.6$ $X(hal,O) = 0.5448$ $X(\delta',O) = 0.5517$	Dataset 2
L → halite + corundum	1873	$X(cor,O) = 0.6$ $X(hal,O) = 0.57$ $X(liq,O) = 0.58$	Wriedt [14]
	1999	$X(cor,O) = 0.6011$ $X(hal,O) = 0.5617$ $X(liq,O) = 0.5584$	Dataset 1
	2012	$X(cor,O) = 0.6000$ $X(hal,O) = 0.5564$ $X(liq,O) = 0.5556$	Dataset 2
L → corundum	2230	–	Wriedt [14]
	2267	–	Dataset 1
	2261	–	Dataset 2
V_3O_5_ht → V_3O_5_lt	428	–	Wriedt [14]
	428	–	Datatset 1
	426	–	Dataset 2
VO_2_ht + L → V_6O_{13}	983	$X(liq,O) = 0.712$	Toda [25]
	982	$X(liq,O) = 0.713$	This work
V_6O_{13} + L → V_3O_7	953	$X(liq,O) = 0.713$	Toda [25]
	950	$X(liq,O) = 0.713$	This work
L → V_3O_7 + V_2O_5	948	$X(liq,O) = 0.713$	Toda [25]
	949	$X(liq,O) = 0.713$	This work
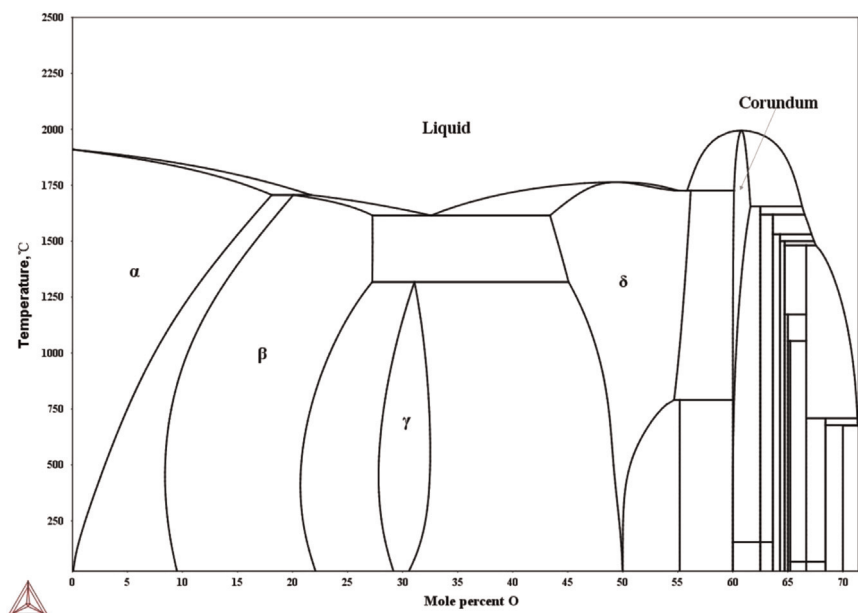
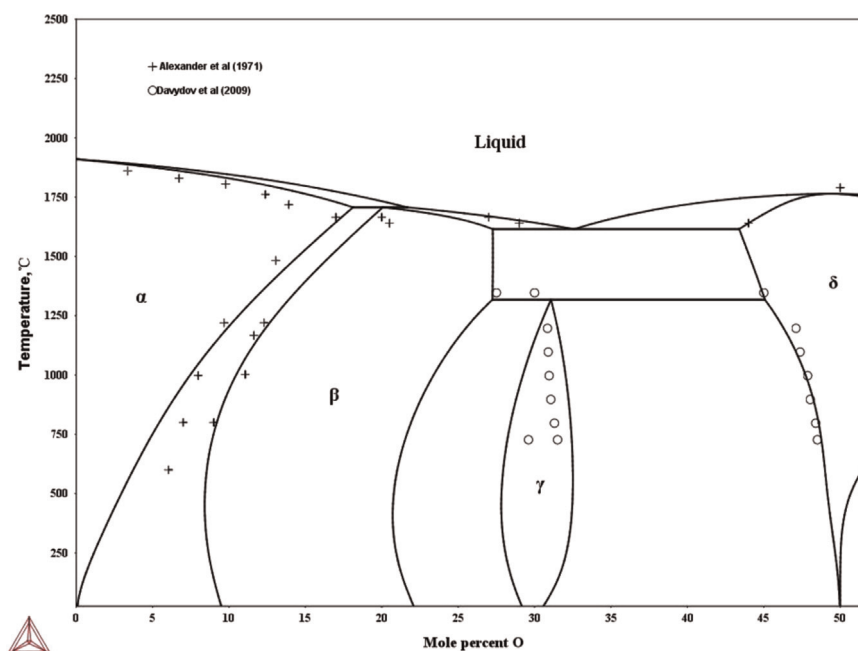**Fig.2.** Calculated V–O phase diagram according to this assessment.

Fig. 3. Part of the V–O phase diagram at lower oxygen content with experimental data.

5.1. Phase diagram

The complete phase diagram with the gas phase suspended is shown in Fig. 2, which is plotted using mole percent *vs.* temperature. It should be kept in mind that the liquid phase is defined up to the composition corresponding to the stoichiometry of V_2O_5 (around 71.43 at% oxygen), which means that the liquidus line becomes unreasonable at higher oxygen contents beyond V_2O_5 where O_2 gas instead of O liquid is stable. Table 2 compares the calculated phase equilibria with experimental data. The present descriptions reproduce the invariant equilibria convincingly well.

Fig. 3 shows a close-up of the phase diagram at lower oxygen content. Generally, good agreement was obtained between experimental and assessed data. The $L+\alpha \rightarrow \beta$ equilibrium shows a discrepancy between measured and calculated data, 42 K in temperature. This could be fitted better if more interaction parameters in the liquid phase were introduced, such as $^2L_{V^{+2}:O^{-2},Va}^{ion}$, which is considered to be somewhat excessive here as the experimental data for liquid is lacking. Furthermore, the exact position of the oxygen-rich boundary of the β-phase is still uncertain. The terminal oxygen solubility in the α-phase was investigated in these studies [16–19,54,55] with lacking consensus. The discrepancy here at temperatures lower than 1073 K is within the
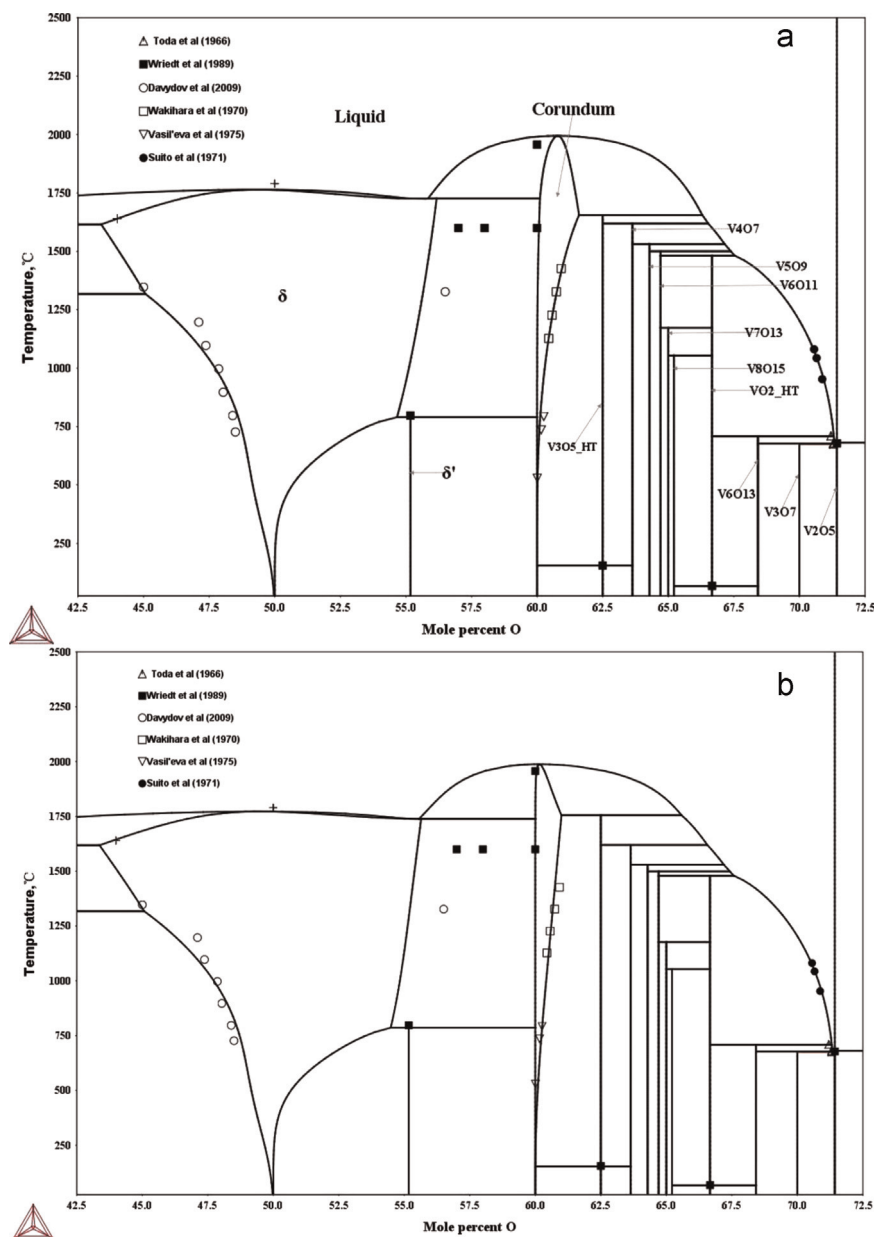
Fig.4. Part of the V–O phase diagram at higher oxygen content with experimental data ((a) is calculated by dataset 1 and (b) by dataset 2).

experimental uncertainties. The calculated solidus of the α-phase is slightly higher than the data from [17]. It was found impossible to fit this information together with the oxygen solubility. It seems that their method [17] of observing the specimen in an optical pyrometer during heating was not sufficiently accurate in this case.

Alexander [17] proposed the peritectoid reaction β+δ→γ at 1458 K while Davydov [53] suggested a higher temperature, 1620 K. The latter experimental information was taken into account here and is well reproduced. More and conclusive measurements are required regarding the homogeneity and stability of the γ-phase.

Fig.4 compares the O-rich portion of the phase diagram with experimental data. It is seen that both of the two datasets can reproduce the experimental information very well. The agreement between different experimental data is convincingly good. The calculated eutectic temperature of L→δ +corundum deviates

from Wriedt's [14] data. It was found impossible to fit both this three-phase equilibrium and the congruent melting point of corundum at the same time. Considering that the temperature of this invariant equilibrium is uncertain according to Wriedt [14], the present deviation is fairly acceptable. The calculated oxygen solubility in the halite phase is lower than the experimental data, which is due to a compromise with other experimental data. Any attempt to improve the fit to this solubility data will have to pay the price for a less satisfactory local optimization, especially the oxygen potential in the halite phase region and the eutectic temperature for L+δ+corundum. More discussions for both halite and corundum will be given in the following sections.

5.2. Liquid phase

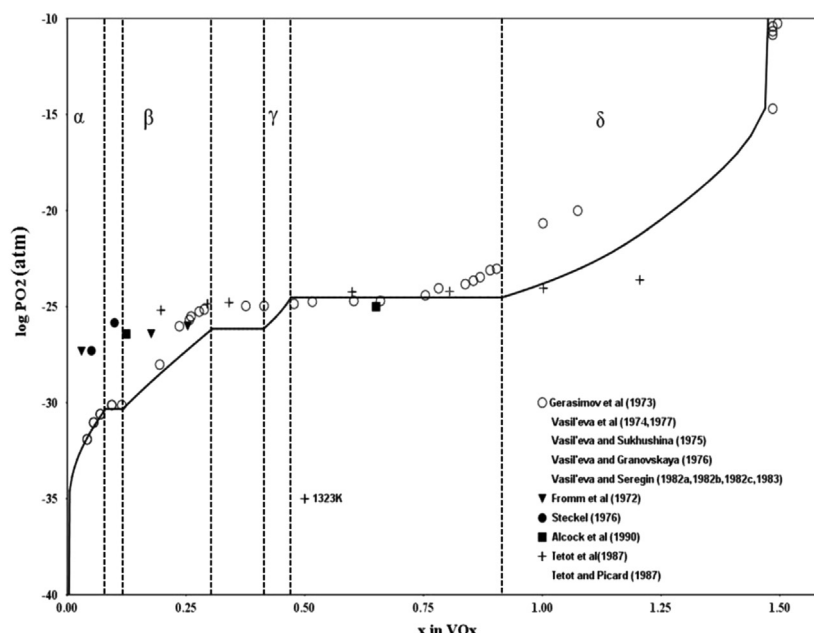Most of the liquidus curves are experimentally speculative

Fig.5. Calculated equilibrium oxygen partial pressure *vs.* oxygen content at 1273 K compared with experimental data. (Data at 1323 K are also appended here using legend "+").

apart from the portions near the invariant reactions and on the VO$_2$-liquidus [27]. The melting points of the δ-phase and the corundum phase together with the former experimentally determined portions (invariant points and the VO$_2$ liquidus) were optimized in the present work. No thermochemical data is available for the liquid phase.

5.3. Solid phases

5.3.1. α, β and γ

A comparison between calculated and experimental oxygen partial pressure at 1273 K which is expressed as log P_{O2} is shown in Fig. 5. It is obvious that a discrepancy exists in experimental data for the homogeneous α, β and δ solid solutions. The present results agree generally well with those from references [20,32–34,47,56–60] for the α and γ+δ phase regions. The deviation in β and β+γ phase regions is probably due to the presently used phase boundary data which is the most updated from Davydov [53]. As the phase boundaries of β and γ are still not well established, more experimental data for these phases are required. The present descriptions for β and γ are further verified to be reliable by reproducing well fitted formation Gibbs energy data shown in Fig. 6. Brewer et al. [41] critically evaluated the formation Gibbs energy of β and γ phases in the temperature range of 1120–1380 K. It can be seen that the calculated and experimental data agree well in the above temperature range.

5.3.2. Halite

The halite model was altered several times before the present one with its parameters was chosen in order to avoid any excessive parameter. A satisfactory phase boundary towards lower oxygen content was obtained by using $L_{V,V^{+2}:O^{-2},Va}^{Hal}$ while $L_{V^{+2},V^{+3}:O^{-2}}^{Hal}$ was adjusted to fit the oxygen-rich phase boundary. Strict control was applied by giving a large positive value to $L_{V^{+3}:O^{-2},Va}^{Hal}$ to have a reasonable variation of the fraction of the species. Fig. 7 shows the calculated site occupancy of all constituents at 1473 K.

It can be seen that V^{+2} and O^{-2} are the dominant species in

the homogeneity range, $x(O)$ from 0.4633 to 0.5517, of the halite phase at this temperature. With the increase of the O content in the range of $x(O) > 0.5$, *i.e.* more O is dissolved into the VO halite, V^{+2} is rapidly replaced by V^{+3} which reflects the oxidation environment at O-sufficient conditions. On the other hand, with the decrease of the O content in the range of $x(O) < 0.5$, *i.e.* more V is dissolved into the VO halite, V^{+2} is mainly replaced by V, which reasonably well reflects the reduction environment at O-deficient conditions. The site fractions of vacancies on both sublattices reach 11.6 at% at the equiatomic composition. Such a vacancy content is comparable to that from [61]. Davydov [61] found that cubic vanadium monoxide contains up to 10–15 at% of structural vacancies in the vanadium and oxygen sublattices simultaneously. It is also evident that the present description for halite reproduces a fairly reasonable oxygen potential in the solution phase region in Fig. 5 within the experimental discrepancy.

5.3.3. Corundum

Thermodynamic description of V$_2$O$_3$ originally taken from SSUB5 database for corundum was optimized in this work together with the related parameter in the liquid phase to fit the congruent melting data. Therefore, it is essential to check the heat contents of the present corundum. It is presented in Fig. 8 that the calculated heat contents are well fitted to the experimental data.

Furthermore, the calculated formation Gibbs energy of corundum by both dataset 1 and 2 agree well with the experimental data from Anderson [62] in Fig. 6.

5.3.4. Stoichiometric phases

Few reliable phase diagram data are explicitly available for the Magnéli phases. Thus, the main attention was paid to optimize the thermodynamic properties of these homologous phases. Table 3 tabulates the data for the enthalpy of formation of Magnéli phases, V$_3$O$_7$ and V$_6$O$_{13}$ at 298.15 K. It shows that the present calculated data are in good agreement with both experimental and previous assessed data.

Table 4 lists entropy data of the Magnéli phases at 298.15 K. The assessed data from both Brewer [41] and Vasil'eva et al. [40] are based on high-temperature equilibrium data due to the lack of
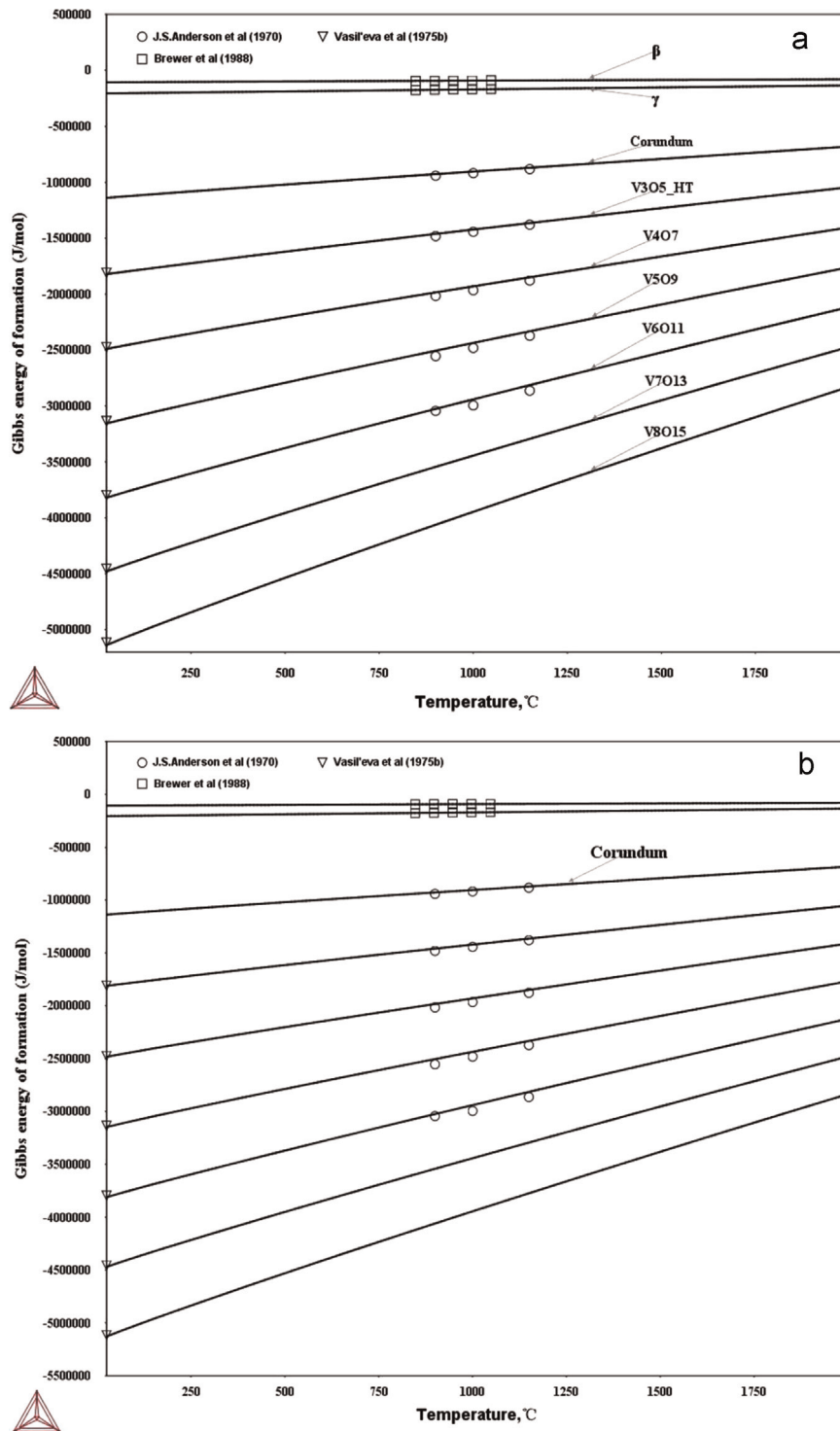
Fig.6. Gibbs energy of formation of several solid phases (values are given in J/mol per formula unit). ((a) is calculated by dataset 1 and (b) by dataset 2).

low-temperature heat capacity values. It shows the present values for the Magnéli phases, V_3O_7 and V_6O_{13} are a bit lower than the extrapolated data from both Brewer [41] and Vasil'eva et al. [40]. The values for V_2O_3, VO_2 and V_2O_5 from different sources are also compared here. An obvious lower value for VO_2 from SSUB5 could be a possible explanation for the lower calculated values for these homologous phases, whose models are based on the descriptions of VO_2 from SSUB5.

Fig. 9 shows a series of equilibrium oxygen partial pressure data expressed as log P_{O2} vs. oxygen content at 1307, 1400, 1473, 1500, 1600 and 1700 K. The agreement between calculated and experimental data for the Magnéli phases is good, which is a further support for the present description.

It is noticed in Fig. 9 that the agreement between the calculations for corundum from the simple model and the measurements is not satisfactory. The reason for this was mentioned in the model
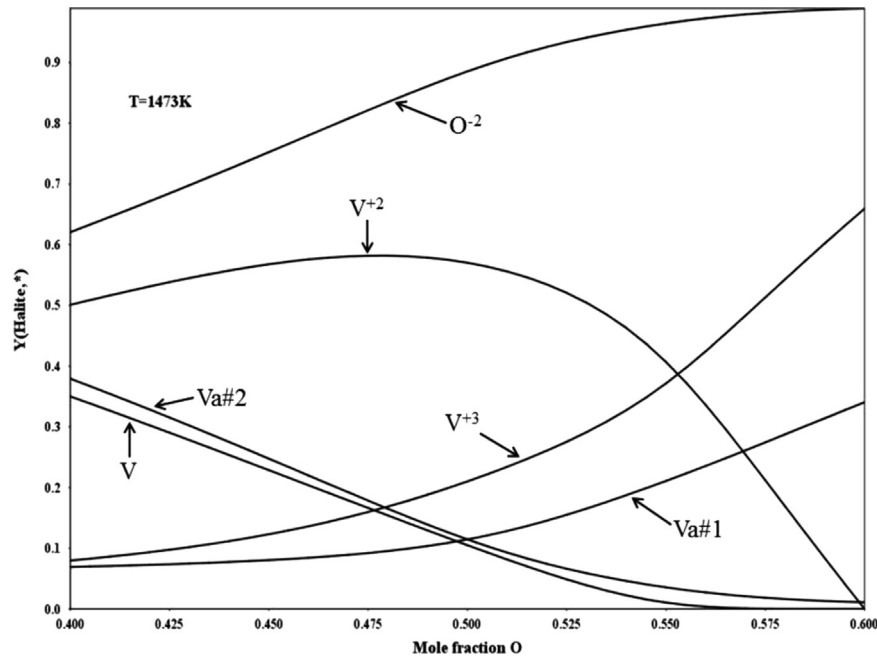
Fig. 7. Calculated site fractions of the species in halite *vs.* *x* (O) at 1473 K.
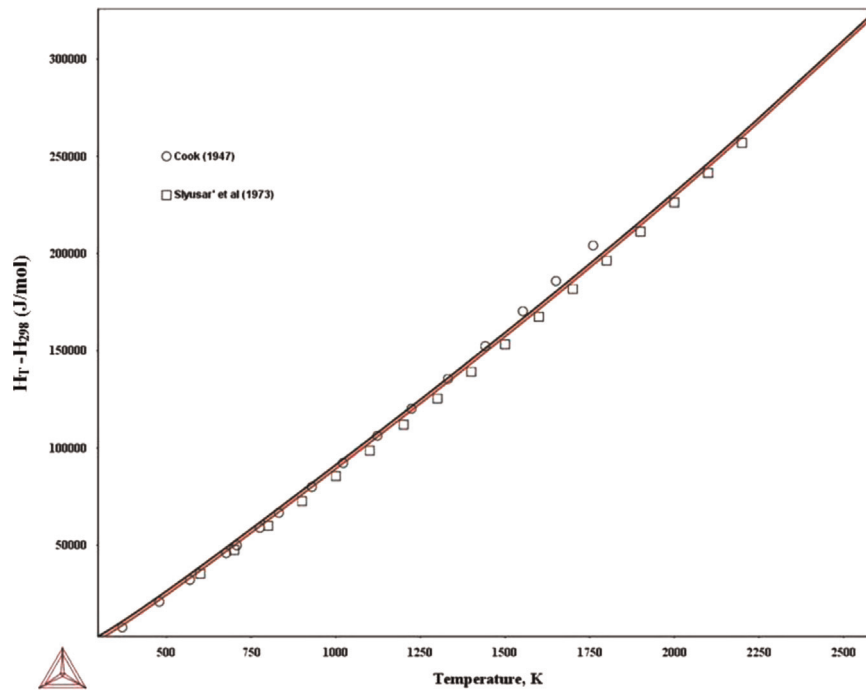

Fig. 8. Calculated heat contents of one mole V_2O_3 corundum compared with experimental data. (Red line is calculated by dataset 1 and black line by dataset 2). (For interpretation of the references to color in this figure legend, the reader is referred to the web version of this article.)

section. Fig. 10 illustrates the corresponding calculations from the advanced model which reproduces the experimental data reasonably well.

The calculated site occupancy of all constituents in corundum by the advanced model at 1900 K is shown in Fig.11. It can be seen that the mole fraction of O^{-2} species on the third sublattice *i.e.* *y* (corundum,O^{-2}#3) is increasing with the increase of the O content which reflects the extra oxygen dissolves in the

interstitial sites. Meanwhile, V^{+2} and V^{+3} are replaced by V^{+4}. It's worth noting that the mole fraction of vacancies on the first sublattice, *i.e.* *y* (corundum, Va#1) keeps at 0 in the whole composition range of corundum, which indicates the defect mechanism is mainly excess oxygen. Therefore, it is reasonable to delete vacancy from the first sublattice in the advanced model. Attempts were made to do so in the present work, and the same fit could be obtained for both phase diagram and equilibrium

Table 3
Enthalpy of formation of Magnéli phases, V_3O_7 and V_6O_{13}.

$\Delta_f^0 H_{298}$(kJ/mol of atoms)	Method	Reference
V_3O_5_LT		
−242.350	Assessed	Brewer [41]
−247.43	Experiment	Charlu and Kleppa [63]
−243.920	Assessed	Dataset 1
−243.951	Assessed	Dataset 2
V_4O_7		
−241.52	Assessed	Brewer [41]
−244.648	Experiment	Charlu and Kleppa [63]
−243.175	Assessed	Dataset 1
−243.199	Assessed	Dataset 2
V_5O_9		
−240.84	Assessed	Brewer [41]
−242.40	Experiment	Charlu and Kleppa [63]
−242.532	Assessed	Dataset 1
−242.550	Assessed	Dataset
V_6O_{11}		
−240.38	Assessed	Brewer [41]
−241.09	Experiment	Charlu and Kleppa [63]
−242.074	Assessed	Dataset 1
−242.088	Assessed	Dataset 2
V_7O_{13}		
−239.79	Assessed	Brewer [41]
−241.486	Assessed	Dataset 1
−241.499	Assessed	Dataset 2
V_8O_{15}		
−239.65	Assessed	Brewer [41]
−238.67	Experiment	Charlu and Kleppa [63]
−241.029	Assessed	Dataset 1
−241.040	Assessed	Dataset 2
V_6O_{13}		
−232.95	Assessed	Brewer [41]
−233.301	Assessed	This work
V_3O_7		
−227.76	Assessed	Brewer [41]
−229.135	Assessed	This work

Table 4
Entropies of the Magnéli phases (values are given per mole atoms).

$^0S_{298}$(J/mol K)	Method	Reference
V_3O_5_LT		
18.80	Assessed	Brewer [41]
18.28	Assessed	This work
18.62	Assessed	Vasil'eva et al. [40]
V_4O_7		
18.97	Assessed	Brewer [41]
17.72	Assessed	This work
17.88	Assessed	Vasil'eva et al. [40]
V_5O_9		
19.07	Assessed	Brewer [41]
17.39	Assessed	This work
17.51	Assessed	Vasil'eva et al. [40]
V_6O_{11}		
19.13	Assessed	Brewer [41]
17.17	Assessed	This work
17.28	Assessed	Vasil'eva et al. [40]
V_7O_{13}		
19.18	Assessed	Brewer [41]
17.15	Assessed	This work
17.13	Assessed	Vasil'eva et al. [40]
V_8O_{15}		
19.21	Assessed	Brewer [41]
17.16	Assessed	This work
17.06	Assessed	Vasil'eva et al. [40]
V_6O_{13}		
19.05	Assessed	Brewer [41]
16.42	Assessed	This work
V_3O_7		
18.64	Assessed	Brewer [41]
15.49	Assessed	This work
V_2O_3		
18.93	Assessed	Brewer [41]
18.90	Assessed	SSUB5 database
19.61	Assessed	JANAF tables [64]
VO_2		
19.92	Assessed	Brewer [41]
15.53	Assessed	SSUB5 database
17.25	Assessed	JANAF tables [64]
V_2O_5		
18.69	Assessed	Brewer [41]
18.64	Assessed	SSUB5 database
18.65	Assessed	JANAF tables [64]

oxygen partial pressure data. However, the non-stoichiometry of V_2O_3 towards the oxygen side due to excess oxygen is unique compared other sesquioxides which was reported towards the metal side. The presence of vacancy provides the model compatibility of describing the generic corundum solution phase with various defect mechanisms. Therefore, out of consideration for the compatibility of large databases, a complete set of model parameters is presented including the constituent vacancy on the first sublattice here.

Fig. 12 shows the phase diagram with the logarithm of the oxygen partial pressure and the inverse of the temperature on the axes, where the two-phase regions have become lines. The available experimental data for the equilibria between Magnéli phases are well reproduced by the present model calculation. The same fit can be obtained from the two datasets.

Fig. 13 shows a close-up of the potential phase diagram mainly involving the VO_2_HT, V_6O_{13}, V_3O_7 and V_2O_5 phases. Point A represents the peritectic reaction of VO_2_HT+Liquid→V_6O_{13} while points B and C represent V_6O_{13}+Liquid→V_3O_7 and Liquid→V_2O_5+V_3O_7, respectively. It is seen that the equilibrium between VO_2_HT and V_6O_{13} is well fitted. However, the equilibrium between V_3O_7 and V_2O_5 could not be simultaneously well optimized with the peritectic temperature of V_6O_{13}+Liquid→V_3O_7. At least two factors contribute to this scatter. Measurements in this region between equilibrium of V_3O_7 and V_6O_{13} are

indispensable. Optimization is generally difficult in such a narrow temperature range.

6. Conclusions

In the present study a critical thermodynamic assessment of the vanadium–oxygen system in the whole composition range was performed for the first time. Two different models for the corundum phase are presented. It excellently reproduces available phase diagram and thermodynamic data within experimental uncertainties. Reasonable attempts were made to avoid excessive number of parameters. The present assessment can be further extrapolated to higher order systems. However, it must be kept in mind that some experimental data are poorly known or largely missing. Most of the liquidus are speculative and the locations of β, γ and δ solid solutions are questionable. No thermochemical data is available for the liquid phase. The lack of consensus on the oxygen potential in the homogeneous α, β and δ solid solutions is striking. The crystal-graphic structures of γ and δ′ are not firmly
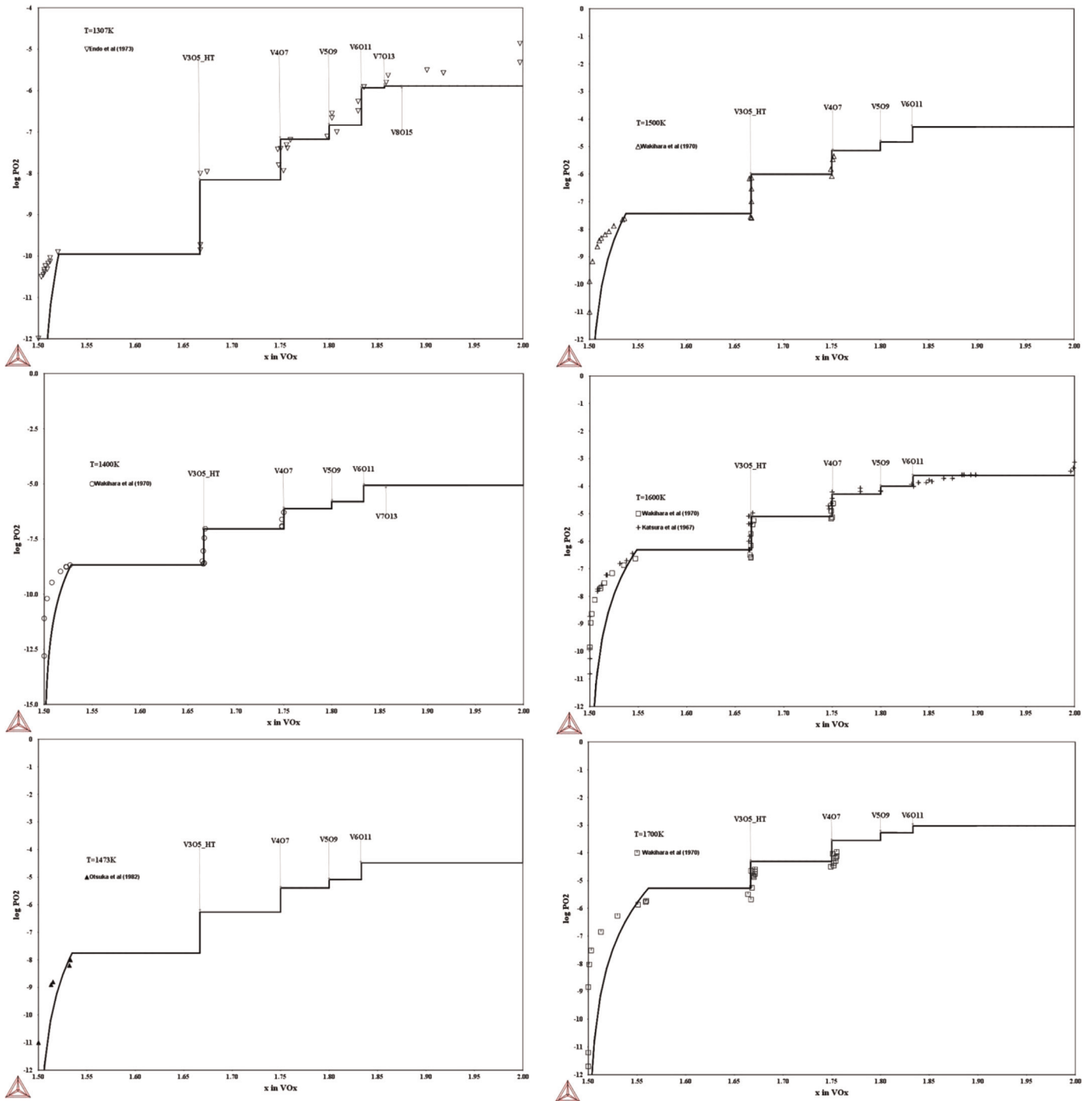
Fig. 9. Calculated equilibrium oxygen partial pressure by dataset 1 of specific phases *vs.* oxygen content at various temperatures compared with experimental data. (The unit for P_{O2} here is atm.).
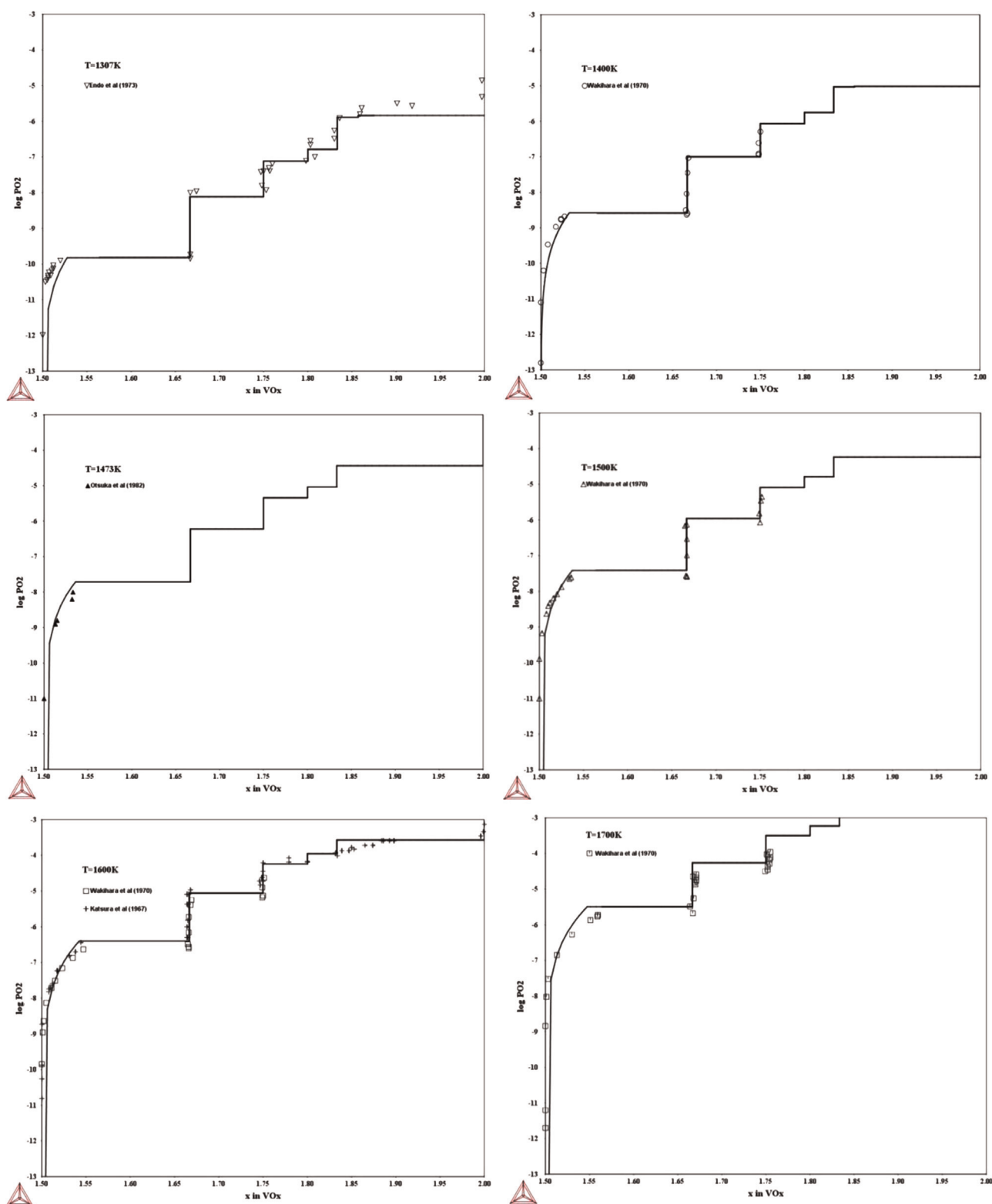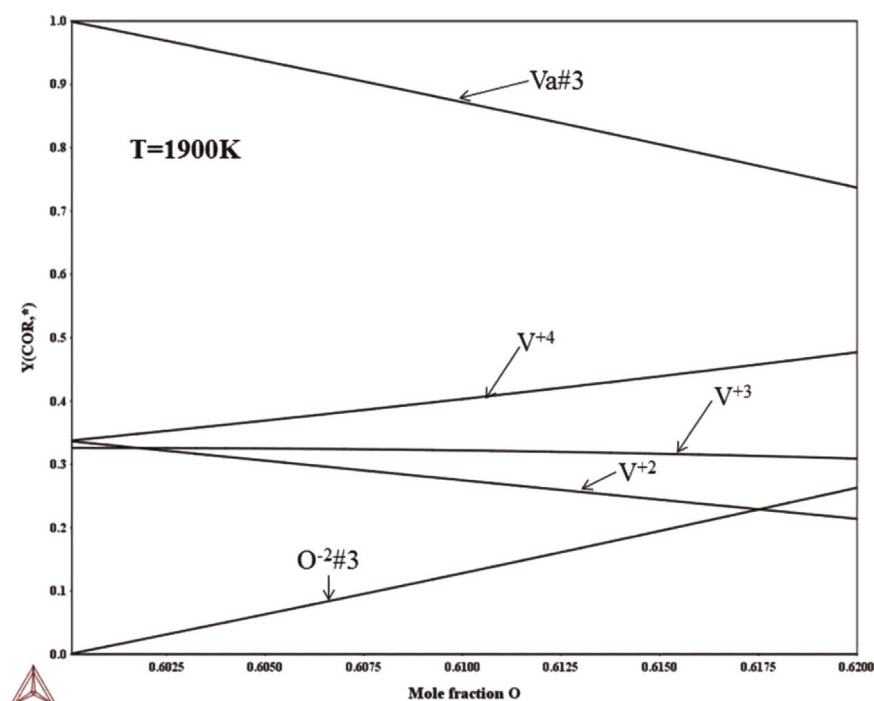
Fig. 10. Calculated equilibrium oxygen partial pressure by dataset 2 of specific phases *vs.* oxygen content at various temperatures compared with experimental data. (The unit for P_{O2} here is atm.).

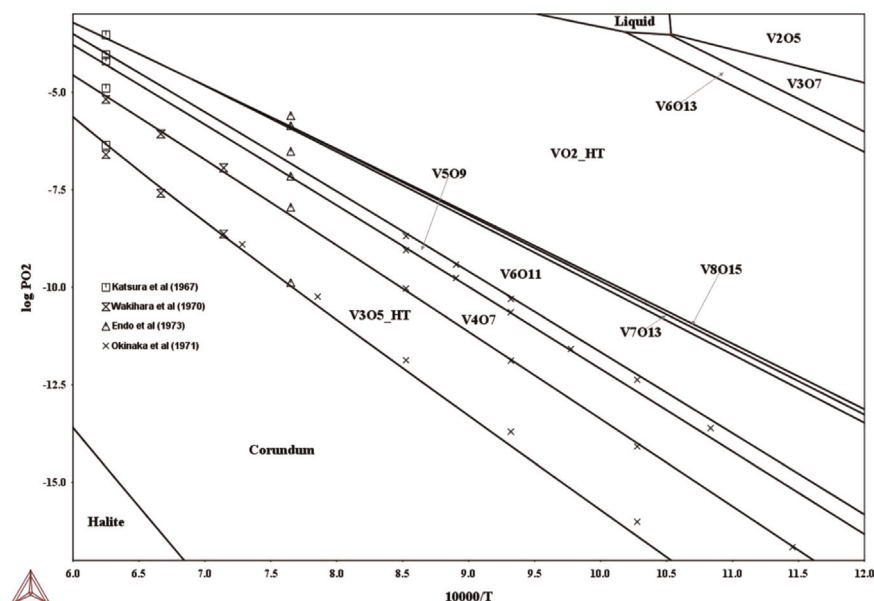**Fig.11.** Calculated site fractions of the species in corundum *vs.* *x* (O) at 1900 K.

Fig. 12. Calculated potential phase diagram of the V–O system on equilibria involving the Magnéli phases. (The unit for P_{O2} here is atm and Kelvin for temperature.).

established. Therefore, further experimental studies on these points are most welcome.

Appendix A. Supplementary material

Supplementary data associated with this article can be found in the online version at http://dx.doi.org/10.1016/j.calphad.2015.08.003.
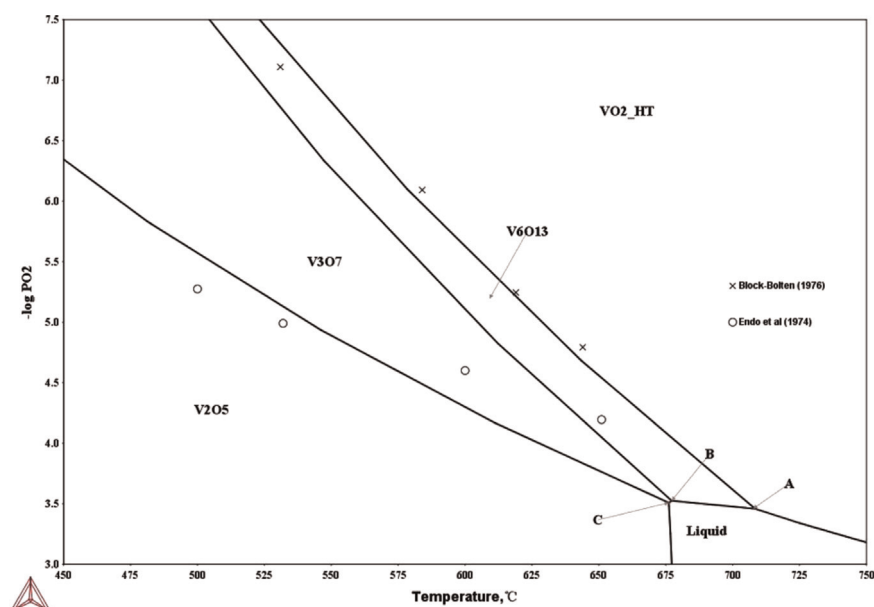
Fig. 13. Part of the potential phase diagram at higher oxygen partial pressure.

References

[1] Banchorndhevakul Weerachai, Matsui Tsuneo, Naito Keiji, J. Nucl. Sci. Technol. 23 (1986) 602–611.
[2] N. Saunders, L. Chandrasekaran, J. Phase Equilib. 13 (1992) 612–619.
[3] Youn-Bae Kang, J. Eur. Ceram. Soc. 32 (2012) 3187–3198.
[4] M. Hillert, B. Jansson, B. Sundman, J. Ågren, Metall. Trans. A 16 (1985) 261–266.
[5] B. Sundman, CALPHAD 15 (1991) 109–119.
[6] M. Selleby, Metall. Trans. B 28 (1997) 563–576.
[7] J. Miettinen, B. Hallstedt, CALPHAD 22 (1998) 257–273.
[8] I. Ansara, N. Dupin, H.L. Lukas, B. Sundman, J. Alloy. Compd. 247 (1997) 20–30.
[9] Q. Chen, B. Sundman, J. Phase Equilib. 19 (1998) 146–160.
[10] H. Mao, M. Selleby, CALPHAD 31 (2007) 269–280.
[11] D. Dilner, H. Mao, M. Selleby, CALPHAD 48 (2015) 95–105.
[12] M. Hillert, S. Jonsson, Metall. Trans. A 23 (1992) 3141–3149.
[13] M. Hillert, J. Alloy. Compd. 320 (2001) 161–176.
[14] H.A. Wriedt, Bull. Alloy Phase Diagr. 10 (1989) 271–277.
[15] Charles B. Alcock, Chunlin Ji, High Temp.-High Press. 22 (1990) 139–147.
[16] J.L. Henry, S.A. O'Hare, R.A. McCune, M.P. Krug, J. Less-Common Met. 21 (1970) 115–135.
[17] D.G. Alexander, O.N. Carlson, Metall. Trans. B 2 (1971) 2805–2811.
[18] E. Fromm, R. Kirchheim, J. Less-Common Met. 26 (1972) 403–406.
[19] G.L. Steckel, C.J. Altstetter, Acta Metall. 24 (1976) 1131–1136.
[20] I.A. Vasil'eva, A.N. Seregin, Russ. J. Phys. Chem. 56 (1982) 945.
[21] P.S. Bell, M.H. Lewis, Phys. Status Solidi A 7 (1971) 431–439.
[22] E. Friederich, L. Sittig, Z. Anorg. Allg. Chem. 145 (1925) 127–140.
[23] W. Klemm, P. Pirscher, Optik 3 (1948) 75–80.
[24] G. Andersson, Research 6 (1953) 45s–46ss.
[25] T. Toda, K. Kosuge, S. Kachi, Nippon Kagaku Zasshi 87 (1966) 1311–1314.
[26] S. Kachi, R. Roy, Techrep Penn State University, 1966.
[27] H. Suito, D. Gaskell, Metall. Trans. 2 (1971) 3299–3303.
[28] O.A. Cook, J. Am. Chem. Soc. 69 (1947) 331–333.
[29] Y. Makakhov, G. Samsonov, Poroshk. Metall. 6 (1966) 84–91.
[30] R. Tetot, C. Picard, J. Solid State Chem. 66 (1987) 324–331.
[31] R. Tetot, C. Picard, P. Gerdanian, J. Solid State Chem. 68 (1987) 88–93.
[32] I.A. Vasil'eva, A.N. Seregin, Russ. J. Phys. Chem. 56 (1982) 986.
[33] I.A. Vasil'eva, A.N. Seregin, Russ. J. Phys. Chem. 56 (1982) 837.
[34] I.A. Vasil'eva, A.N. Seregin, Russ. J. Phys. Chem. 57 (1983) 987.
[35] M. Wakihara, T. Katsura, Metall. Trans. 1 (1970) 363–366.
[36] T. Katsura, M. Hasegawa, Bull. Chem. Soc. Jpn. 40 (1967) 561–569.
[37] H. Endo, M. Wakihara, M. Taniguchi, T. Katsura, Bull. Chem. Soc. Jpn. 46 (1973) 2087–2090.
[38] N. Otsuka, H. Sato, G.L. Liedl, J.M. Honig, J Solid State Chem. 44 (1982) 230–244.
[39] N. Slyusar', A. Krivorotenko, E.N. Fomichev, A. Kalashnik, V. Bondarenko, Russ. J. Phys. Chem. 47 (1973) 1525.
[40] I.A. Vasil'eva, I.S. Sukhushina, R.F. Balabaeva, J. Chem. Thermodyn. 7 (1975) 319.
[41] Leo Brewer, Bartley B. Ebbinghaus, Thermochim. Acta 129 (1988) 49–55.
[42] M. Temkin, Acta Phys. Chim. USSR 20 (1945) 411–417.
[43] Rainer Mittelstädt, Klaus Schwerdtfeger, Metall. Trans. B 21 (1990) 111–120.
[44] B. Sundman, J. Phase Equilib. 12 (1991) 127–140.
[45] H. Ohtani, M. Hillert, CALPHAD 14 (1990) 289–306.
[46] K. Hiraga, M. Hirabayashi, Trans. Jpn. Inst. Met 16 (1975) 431–440.
[47] I. Vasil'eva, I. Sukhushina, J Chem Thermodyn. 7 (1975) 5–12.
[48] B. Andersson, J. Gionnes, Acta Chem. Scand. 24 (1970) 2250–2252.
[49] M. Morinaga, J.B. Cohen, Acta Crystallogr. Sect. A: Cryst. Phys. Diffr. Theor. Gen. Crystallogr. 35 (1979) 745–756.
[50] J.M. Thomas, Eur. J. Solid State Inorg. Chem. 31 (1994) 651–661.
[51] Leslie Glasser, Inorg. Chem. 48 (2009) 10289–10294.
[52] J.-O. Andersson, T. Helander, L. Höglund, P. Shi, B. Sundman, CALPHAD 26 (2002) 273–312.
[53] D.A. Davydov, A.A. Rempel, Inorg. Mater. 45 (2009) 47–54.
[54] D.L. Smith, J. Less-Common Met. 31 (1973) 345–358.
[55] J.L. Henry, S.A. O'Hare, R.A. McCune, Marion P. Krug, J. Less-Common Met. 21 (1970) 115–135.
[56] Y.I. Gerasimov, I.A. Vasil'eva, R.F. Balabaeva, Dokl. Akad. Nauk SSSR 211 (1973) 98.
[57] I.A. Vasil'eva, Zh.V. Granovskaya, I.S. Sukhushina, Russ. J. Phys. Chem. 48 (1974) 904.
[58] I.A. Vasil'eva, Zh.V. Granovskaya, A.N. Seregin, Russ. J. Phys. Chem. 51 (1977) 1228.
[59] I.A. Vasil'eva, Zh.V. Granovskaya, Russ. J. Phys. Chem. 50 (1976) 876.
[60] C.B. Alcock, J.C. Chan, 1990, unpublished work.
[61] D.A. Davydov, A.I. Gusev, JETP Lett. 91 (2010) 286–291.
[62] J.S. Anderson, A.S. Khan, J. Less-Common Met. 22 (1970) 209–218.
[63] T.V. Charlu, O.J. Kleppa, High Temp. Sci. 5 (1973) 260.
[64] JANAF, Thermodynamical Table, 3rd, 1985, pp. 1702, 1712, 1722.
[65] H. Okinaka, K. Kosuge, Trans. Jpn. Inst. Met. 12 (1971) 44–48.
[66] A. Block-Bolten, Can. J. Chem. 54 (1976) 1967–1970.
[67] H. Endo, M. Wakihara, M. Taniguchi, Chem. Lett. 3 (1974) 905–908.